UNCLASSIFIED

AD 296 367

Reproduced
by the

ARMED SERVICES TECHNICAL INFORMATION AGENCY
ARLINGTON HALL STATION
ARLINGTON 12, VIRGINIA

UNCLASSIFIED

NOTICE: When government or other drawings, specifications or other data are used for any purpose other than in connection with a definitely related government procurement operation, the U. S. Government thereby incurs no responsibility, nor any obligation whatsoever; and the fact that the Government may have formulated, furnished, or in any way supplied the said drawings, specifications, or other data is not to be regarded by implication or otherwise as in any manner licensing the holder or any other person or corporation, or conveying any rights or permission to manufacture, use or sell any patented invention that may in any way be related thereto.

03-2-4

CATALOGED BY ASTIA
AS AD No. 296367

CONTRACT NO. AF33(657)8490
BPS NUMBER 2)63-699-750F-817301-16)
TASK NO. 817301-16

APPLIED RESEARCH PROGRAM ON HIGH-TEMPERATURE RADIATION-RESISTANT SOLAR-CELL ARRAY

QUARTERLY TECHNICAL PROGRESS REPORT NO. 3
NOVEMBER 1962 – JANUARY 1963

296 367

Prepared for the

U.S. AIR FORCE
AERONAUTICAL SYSTEMS DIVISION
WRIGHT-PATTERSON AFB, OHIO

By the

ASTRO-ELECTRONICS DIVISION
DEFENSE ELECTRONIC PRODUCTS
RADIO CORPORATION OF AMERICA
PRINCETON, NEW JERSEY

ASTIA
FEB 18 1963

AED 1816

Issued: January 31, 1963

The work covered by this report was accomplished under Air Force Contract No. AF33(657)-8490, but this report is being published and distributed prior to Air Force Review. The publication of this report, therefore, does not constitute approval by the Air Force of the findings or conclusions contained herein. It is published for the exchange and stimulation of ideas.

TABLE OF CONTENTS

TABLE OF CONTENTS (Continued)

LIST OF ILLUSTRATIONS

LIST OF ILLUSTRATIONS (Continued)

LIST OF TABLES

APPLIED RESEARCH PROGRAM ON HIGH-TEMPERATURE RADIATION-RESISTANT SOLAR-CELL ARRAY

QUARTERLY TECHNICAL PROGRESS REPORT NO. 3

NOVEMBER 1962 - JANUARY 1963

I. SUMMARY OF WORK ACCOMPLISHED

A. Gallium Arsenide Cell Development and Fabrication

1. Cell Production

During the third quarter, a total of 326 gallium arsenide cells were fabricated to meet the needs of the various temperature, radiation, and array design tests. A graph of frequency distribution versus cell efficiency for the third quarter is shown in Figure 1. A significant point is that during this period, the pilot line production peaked at a cell efficiency of about 8 percent. When this is compared with the peaks of the distributions for the first and second quarters production shown in Figures 2 and 3, it can be seen that a progressive improvement in the typical cell efficiency has been accomplished. Between the first and third quarters, the shift of the peak efficiency from 7 percent to 8 percent amounts to a net improvement of more than 14 percent. The factors contributing to this advancement are improvements made in every step of the process including operator supervision.

Figure 4 shows a graph of frequency distribution versus cell efficiency for the total pilot line production through the third quarter.

2. Cell Measurements (Electrical)

A solar cell is generally characterized electrically by the conversion efficiency, which is defined as the ratio of the maximum available power to the total radiant power incident on the active area. The conversion efficiency is determined from the current-voltage curve recorded under a tungsten light source whose intensity is adjusted to produce a specified short-circuit current on a "standard solar cell."

The specified short-circuit current of the standard solar cells is determined from sunlight measurements of short-circuit current, during which the total solar radiation is measured using an Eppley Normal Incidence Pyrheliometer. These measurements

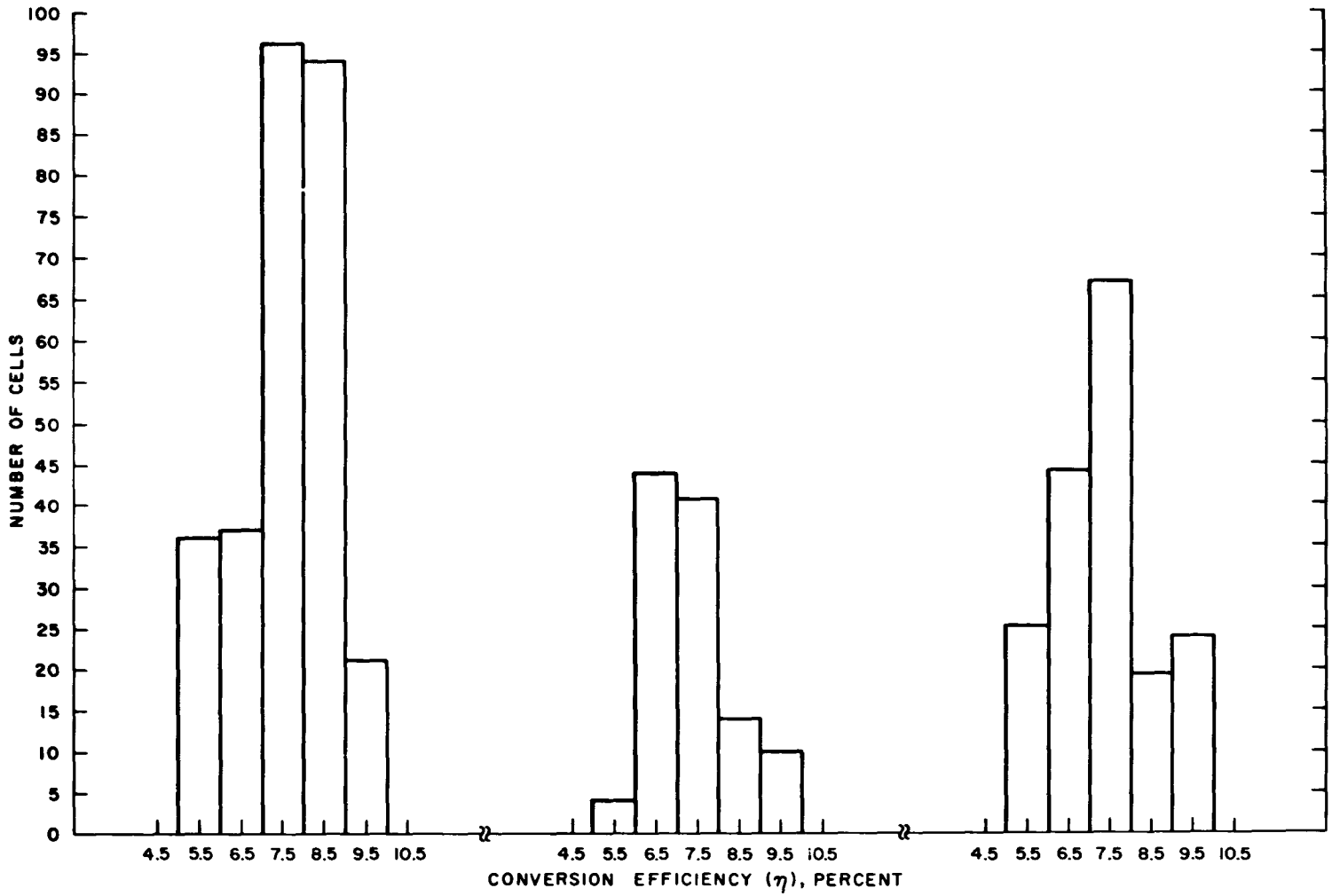

Figure 1. Third-Quarter Pilot Line Production

Figure 2. First-Quarter Pilot Line Production

Figure 3. Second-Quarter Pilot Line Production

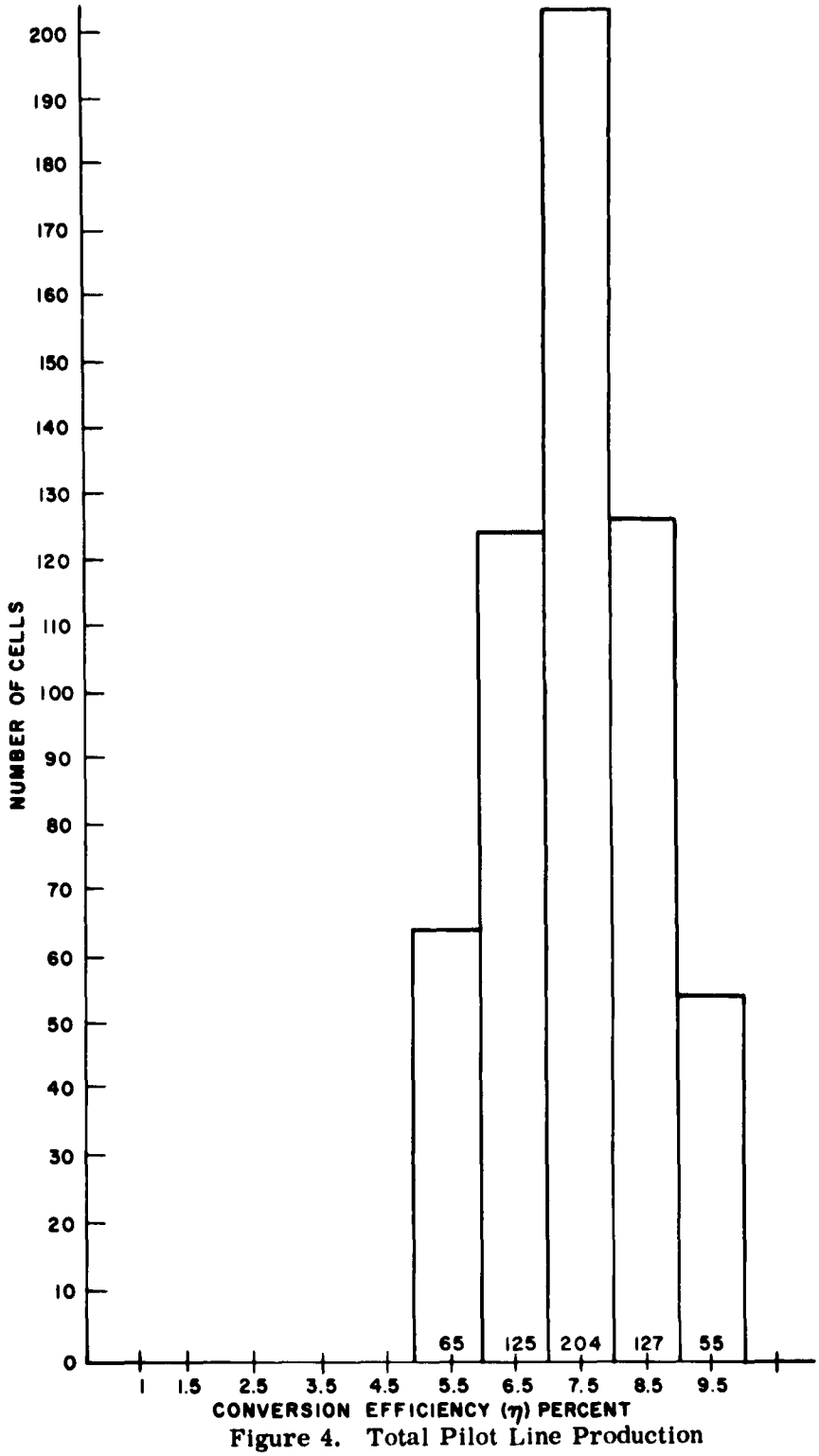

Figure 4. Total Pilot Line Production

are made only on clear, bright days in the absence of haze and visible clouds. If these conditions prevail, and the measured solar irradiation is greater than 90 milliwatts per square centimeter, the measured short circuit current is extrapolated linearly to 100 milliwatts per square centimeter. This level of solar radiation was selected for in-process testing because it is approximately the value reported by Moon (see Reference 1) for the maximum sunlight reaching the earth's surface, and because it is a value used by many researchers.

As previously indicated in Quarterly Technical Progress Report No. 2, two methods of predicting the short-circuit current of solar cells outside the earth's atmosphere are being explored. These methods are discussed in detail below.

The first method, proposed by Zoutendyk (see Reference 2) is based upon the well known relation for exponential attenuation of monochromatic light traveling through the atmosphere

$$I_m(\lambda) = I_o(\lambda)\, e^{-\alpha(\lambda)m}, \tag{1}$$

where m is the air mass, defined more fully as the length of the atmospheric path transversed by the sun's rays in reaching the earth's surface, measured in terms of this path when the sun is in the zenith;

$\alpha(\lambda)$ is the atmospheric absorption coefficient;

λ is the incident light wavelength;

$I_o(\lambda)$ is the unattenuated light intensity; and

$I_m(\lambda)$ is the intensity at a given air mass.

The short-circuit current, generated by monochromatic light, has the same form as equation (1). It does not follow that the total short-circuit current will have a similar form however, because of the nonlinear dependence of current on wavelength. Experimental data presented in reference 2, however, demonstrates that a semilogarithmic plot of the short-circuit current at a given air mass (I_{scm}) versus air mass (m) describes a straight line for air mass less than 3. Thus, based upon these results, it is possible to write

$$I_{scm} = I_{sco}\, e^{-\alpha m} \quad \text{for } m < 3, \tag{2}$$

where I_{scm} is the total collimated short-circuit current at air mass m and I_{sco} is the total collimated short-circuit current at air mass zero. In order to apply this information, it must be possible to calculate the air mass from the location of the testing

station, the date, and the local standard time of a sunlight measurement of short-circuit current. This may be done from published data (see Reference 3) as follows. The angles measured from the vertical and the horizontal to the direction of the sun's incident rays are the zenith (z) and altitude (a) of the sun, respectively. From this geometry and from the definition of air mass, it is apparent that for zenith angles less than 70° (for which atmospheric refraction effects are negligible), the following relation holds.

$$m = \sec z = \frac{1}{\sin a} \tag{3}$$

The altitude of the sun is found from the equation

$$\sin a = \sin \varphi \sin \delta - \cos \varphi \cos \delta \cos h, \tag{4}$$

where a is the altitude of the sun;

φ is the latitude of the test station;

δ is the declination of the sun; and

h is the hour angle of the sun.

The solar declination (δ) is a function of the annual earth orbit. The solar hour angle (h) is the angular distance measured from the meridian of the test station, and is therefore a function of both the annual orbit and daily rotation of the earth. The necessary information for calculating both (δ) and (h) is tabulated in Table 169 of reference 3.

Measurements of the type described above have been made on ten cells selected from the pilot line production. The measurements were made at the RCA Semiconductor and Materials Division (SMD) at Somerville, N.J., during the months of October and November of 1962. Figure 5 shows semilogarithmic plot of Ln I_{scm} versus m for one of the cells. The data shown does not show the linear variation expected. If, however, the data for air mass 1.51 and 1.57 (which was recorded in the presence of some low lying clouds) is disregarded, the three remaining points describe a straight line. Because of the small number and range of data, more measurements will be necessary before any conclusions can be drawn.

The second method of predicting the short-circuit current outside the atmosphere (I_{sco}) depends upon a measurement of the absolute spectral response $S(\lambda)$ of the solar cell. The detailed procedure used in this measurement is described in Technical Documentary Report No. ASD-TDR-62-932. Assuming that one is able to measure

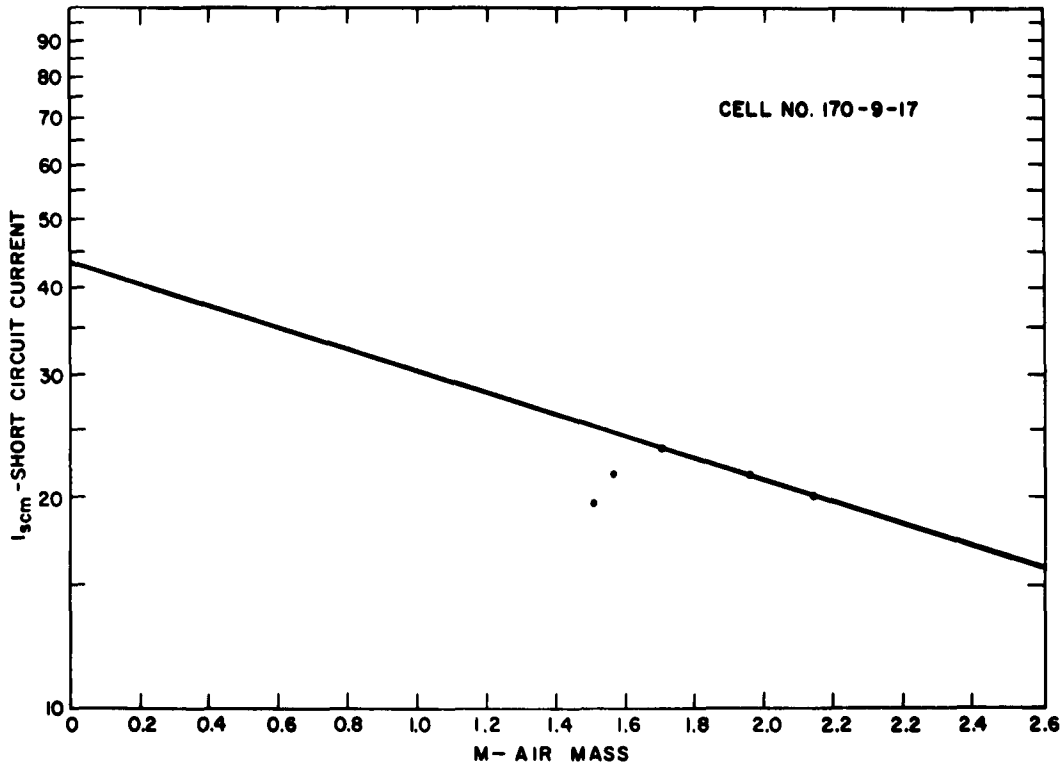

Figure 5. Plot of Ln I_{scm} Versus m

S(λ), it is then possible to graphically evaluate the integral

$$I_{scm} = \int_{\lambda_1}^{\lambda_2} A\, q \left[N_{ph}\,(\lambda)\right]_m S(\lambda)\, d\lambda, \tag{5}$$

where I_{scm} is the short-circuit current at air mass m;

A is the active cell area;

q is the electronic charge; and

$\left[N_{ph}\,(\lambda)\right]_m$ is the number of photons per square centimeter per unit wavelength at air mass m.

Since values of $\left[N_{ph}\,(\lambda)\right]_m$ are available (see Reference 4) for m = 0, the integral may be evaluated to obtain I_{sco}.

3. Efficiency Versus Temperature

The test fixture has been constructed and evaluated for recording the current voltage (I-V) characteristics of solar cells as a function of temperatures between 25°C and 200°C. The initial measurements on 8 of the remaining 25 cells have been taken, and the data is presently being analyzed.

4. Shelf Life of Cells at 200°C

Ten gallium arsenide cells were placed in an environment of 200°C at one-atmosphere pressure, and the current-voltage (I-V) characteristics were measured under a tungsten light source. This test has been run to completion at 1000 hours with measurements at five intervals. In order to eliminate the possible changes due to different standard cells, an eleventh cell was measured in sunlight, stored at room temperature, and used as the "standard" cell for calibrating the light source for all measurements. Five parameters were checked for variations: open-circuit voltage (V_{oc}), short-circuit current (I_{sc}), voltage at the maximum power point (V_{mp}), the current at the maximum power point (I_{mp}), and the conversion efficiency (η). The test results are presented in Table I.

TABLE I.

GALLIUM ARSENIDE CELL TEST RESULTS

Cell No.	Original η	Percent Change				
		I_{sc}	V_{oc}	I_{mp}	V_{mp}	η
1	7.5	-2.6	0	- 2.5	+2.2	- 0.3
2	6.2	-2.4	0	- 0.3	-1.6	- 1.9
3	7.3	-1.4	0	- 0.5	0	+ 0.6
4	6.9	-1.5	0	0	+2.9	+ 2.9
5	8.1	-1.3	- 1.1	- 2.9	+0.7	- 2.2
6	6.4	-4.0	0	- 2.3	+0.8	0
7	7.5	-2.9	- 1.7	- 2.6	-3.6	- 5.6
8	7.6	-3.8	- 1.2	- 3.3	+2.3	- 5.7
9	6.9	-3.2	+22.9	- 1.0	+5.7	+ 4.5
10	7.9	-3.3	- 1.2	-19.3	-7.8	-25.6

During the test, two changes became apparent in the lead solder: it became heavily oxidized, and it showed some internally originating blisters. The oxidation is expected with lead contacts in air at 200°C; the blisters may be due to flux trapped during cell fabrication. In order to insure good electrical contact during measurement of the I-V characteristics, the solder was mechanically abraded after removal from the test atmosphere.

The total experimental error for these measurements is estimated at about 5 percent. The catastrophic failure of cell No. 10 occurred during the first 300 hours of the test and is unexplained. Note that the changes in I_{sc} and I_{mp} were all negative, while those in the other three parameters were both positive and negative. This latter (the variation in parameters), indicates that the small degradation in current may be a true phenomenon and not a systematic error. The maximum change of 4 percent of I_{sc} (excluding No. 10) does not appear to be extremely serious.

5. Silicon Monoxide (SiO) Anti-Reflection Coating

(The work described below was performed under Contract AF33(657)-8921, and has been reported in Status Letter No. 4 of that contract. The results are applicable to this contract and are included for completeness). In order to check the reproducibility in the thickness of the evaporated layer of SiO, a highly polished silicon wafer was placed in each of four different evaporation runs. Next, a thin film of aluminum was evaporated over the wafers and the thickness measured by standard interference microscope technique. The results were as follows:

Lot No.	Thickness
170-28	1080A ± 100A
120-29, 30, 35	1050 ± 100
170-37	1050 ± 100
170-40	1050 ± 100

The results indicate that the method used in normal processing yields excellent control of SiO thickness.

Infrared investigation of the anti-reflection coating revealed that, under normal evaporation conditions, the coating was a mixture of SiO and SiO_2. SiO has an absorption band at 10.0 microns and SiO_2 has one at 9.25 microns. The absorption band for the anti-reflection coating occurred at 9.55 microns.

Several samples of gallium arsenide were prepared and subjected to normal evaporation conditions except that a coating of approximately 1500 A was deposited on them. This deposition results in material thickness as required to facilitate infrared investigation. These wafers were stored at various temperatures and checked periodically to observe the effect of temperature on the stability of the coating. It was observed that a slight shift from 9.55 microns occurred toward 9.25 microns during the first 48 hours of storage at an elevated temperature. However, after 350 hours of storage, no additional shifting took place. The temperatures to which the samples were subjected and the corresponding final absorption bands recorded are as follows:

Temperature	Initial	After 350 Hours
25°C	9.55	9.55
100°C	9.55	9.50
150°C	9.55	9.50
265°C	9.55	9.40

The results indicate that some conversion of SiO to SiO_x occurs during the first 48 hours of temperature storage. Since no major conversion has been disclosed by continued high temperature storage, no further work in this area is planned.

6. References:

(1) Moon, P., Proposed Standard Solar Radiation Curves for Engineering Use, 1940, J. Franklin Institute, 230, 583-617.

(2) Zoutendyk, John A., "A Method for Predicting the Efficiency of Solar Cell Power Systems Outside the Earth's Atmosphere," Proc. of Solar Working Group Conf., Vol. II, February 1962.

(3) Smithsonian Meteorlogical Tables, Sixth Revised Edition, Washington, D.C. 1958.

(4) Wysocki, J.J., "Photon Spectrum Outside The Earth's Atmosphere," Solar Energy, VI, 104, (1962).

B. Array Design and Testing

1. Summary

Two 20-cell panels, one a mechanical sample and the other a 6-percent (efficiency) electrical prototype (each approximately 45 grams in weight) were subjected to the qualification tests described in Exhibit A-1 of the Contract. The tests consisted of: vibration, both sine-wave and random; shock; acceleration; and temperature-launch. The temperature-launch test limits were changed from plus 165 - minus 30 degrees F to plus 200 - minus 40 degrees F as a result of a meeting at the Wright-Patterson Air Force Base during November 1962 (involving AED, Lockheed, contractors, and Air Force personnel). Both panels met the specification requirements without degradation with the exception of a minor assembly defect which occurred on the mechanical sample.

The 6-percent electrical prototype sample was subjected to a thermal-vacuum cycling test in addition to the tests listed previously. A thermal analysis was made of the panel, employing outer-space and orbiting conditions described by the Lockheed Aircraft Corporation; results of this analysis showed the temperature limits to be plus 80 degrees to minus 80 degrees C. In addition to determining the temperature limits, a temperature-time profile was determined. The 6-percent panel was subjected to thermal-vacuum tests simulating the results of the analysis. At the conclusion of 40 cycles, the panel was removed from the test chamber and inspected; approximately 80 percent of the cells had cracked. The data collected during the test was analyzed in detail and indicated that no unusual conditions had occurred which would result in stress in excess of that calculated.

A number of tests were undertaken to discover the cause of the difficulty as a result of the thermal-vacuum test; these are described in detail later in the report. The panel was redesigned at about the same time as these tests. The purpose of the redesign was to raise the low temperature, to reduce the differential between the high and low temperatures, and to reduce the rate of temperature change. These were accomplished by increasing the thermal mass of the panel with a resultant increase in weight to approximately 110 grams. The new temperature limits are plus 82 degrees C and minus 15 degrees C. A sample of the redesigned panel was subjected to 48 cycles of thermal-vacuum tests without degradation.

No additional details of the qualification tests are given in this Report since the entire test program will be repeated for the redesigned (110-gram) panel; additional details of the thermal-vacuum cycling will be given, however.

During this quarter, additional work was done on high-temperature soldering. The techniques developed are sufficiently advanced to permit the use of high-temperature solder for all orbital panels.

2. Array Construction

A number of panels have been built by means of a technique that appears to be satisfactory and has evolved because of the uneven solder backing on the cells. Leads and cells or modules are normally placed on a substrate which is covered to some extent with wet adhesive. However, when this method was first used, the cells cocked in conformance with the uneven solder backing. To achieve a plane surface on the final panel, the technique used consists essentially of holding the cell faces (P side) on a fixture and bonding the substrate to the cells instead of the normally opposite way.

The technique has evolved to the point where a manufacturing specification will be generated if no difficulties arise in environmental testing because of its design or execution.

3. Investigation of Cell Failures During Thermal-Vacuum Testing

a. Tests to Determine Cause of Failures

(1) Quick-Cycle Test

This test was devised to rapidly find corrective action. It consists of cycling cells between minus 70°C and plus 80°C in air, using dry ice as the coolant and lamps for heating. The cells tested were affixed to a thin aluminum sheet with double-faced masking tape. A thermocouple is provided on one of the cells and the assembly is placed in a hollow between blocks of dry ice. When the low temperature is reached, the board is placed under the heat lamps until the high limit is reached.

The above-described test was performed immediately after the thermal-vacuum test during which the failures occurred. The object was to check a number of variables. Four cells of each of the following five types were tested:

1. Cells as received.
2. "Bare" cells, i.e. with no solder applied to ohmic contacts.
3. Low-temperature leads soldered to cells (the type that failed in thermal-vacuum).
4. High-temperature leads soldered to cells.
5. Silicon 2 x 2 cm cells, as a control.

An additional cell of type 1 was added to the center of the board to carry the thermocouple. Approximately 50 cycles were run with cooling rates of 75°C per minute and heating rates of 55°C per minute.

Other than the cell with the thermocouple (which may have cracked while taping the thermcouple to it), the only cracking occurred in types 2 and 3. Two cells in each of these groups cracked between the 13th and 15th cycles. All cells were mechanical samples, i.e. efficiencies of less than 6 percent. The significance of these results is discussed in the next section.

(2) Thermal-Vacuum Test of Unmounted Cells

A thermal-vacuum test was run on "free" cells (no double faced adhesive tape), with different cells of the same types and sample sizes as used in the quick-cycle test. The temperature limits were the same as originally, namely minus 80°C to plus 80°C. No failures (cracking) resulted.

At this point, the differences between the tests should be stated. In the panel test, the cells all had low-temperature leads and were bonded to a substrate. In the quick-cycle test, the cells were affixed to a substrate with a tape whose action under the test conditions is completely unknown. In the "free" test, no constraints were placed on the cells. The panel and "free" tests had heating and cooling rates essentially the same, while the quick-cycle test used much higher rates. The cell efficiencies were low in the quick-cycle and free tests, while the panel test used cells in the 6 to 8-percent range.

(3) Tests of RTV-60 Silicone Rubber Characteristics

Consideration of the room-temperature modulus of elasticity of RTV-60 (approximately 1×10^3) would seem to preclude its ability to either induce or transmit strains to the cells; its modulus at minus 80°C is unknown. To test the hypothesis that the mounting arrangement did not contribute to the cell failures, the following tests were set up:

(a) An aluminum panel 6 inches by 2 inches by 0.062 inches thick was cut and three 1-by-2 cm aluminum chips (cut from the same base sheet) were bonded to it with three different thicknesses of RTV-60. Strain gages were mounted on the chips and on the back of the panel under the chip locations. The panel was then placed in a tension testing machine and loaded in tension. The strain-gage readings indicated that the RTV-60 transmitted no strain to the chips at room temperature while the substrate was in tension (see Table II). In making the set-up, it was found that on occasion, some bending was introduced or present in the thin panel and at least some of this was transmitted through the RTV-60. Since bending of the substrate did not enter the failure picture, this phenomena has not as yet been studied further. If the budget is sufficiently large, this test will be rerun at approximately minus 70°C.

TABLE II. TENSION TEST FOR TRANSMISSIBILITY OF LOADS BY RTV-60

Load (lbs.)	Strain (microinches per mil)				Load (lbs.)	Strain (microinches per mil)			
	4	3	2	1		4	3	2	1
First Run:					Second Run (Cont):				
0	-10	-2	0	0	450	361	0	1	5
10	-12	10	20	15	500	401	0	0	5
50	17	10	19	18	550	450	0	0	2
100	61	10	12	12	600	492	0	0	2
150	102	8	10	10	498	400	0	0	2
200	150	5	9	10	398	319	1	2	2
250	190	3	6	8	299	235	2	7	7
300	235	2	5	8	200	150	8	10	10
350	275	1	2	7	105	63	10	12	12
401	319	0	2	5	50	19	11	19	19
Second Run:									
200	---	8	10	10					
400	---	1	3	5					
500	375	-	-	-					
600	---	0	0	5					
800	625	0	1	6					
1000	---	0	0	2					
1200	965	-2	-3	2					
1400	---	-4	-8	1					
1600	1310	-4	-9	1					
1800	---	-5	-10	0					
2000	1650	-6	-10	0					

Note: 1. Chip No. 1 - RTV-60 thickness: 3 mils
Chip No. 2 - RTV-60 thickness: 16 mils
Chip No. 3 - RTV-60 thickness: 26 mils
Chip No. 4 - Refers to strain gage on back of panel

2. (-) sign indicates compression. Strain rate was 0.01" per minute.

(4) Thermal-Shock Test of Cells at SMD-Somerville

To determine whether an efficiency-linked phenomenon contributing to cracking, a simple test was conducted at Somerville. Liquid nitrogen was poured over a series of low-efficiency cells, each in a Petri dish; none cracked. The test was repeated using 8-percent-efficient cells; three out of four cracked.

(5) Cell Measurements

Measurements were made of cells to check the possibility of bending stresses causing the cracking. The theory is that at the melting point of the solder backing it is assured that the cells are flat and a zero-stress condition prevails. As the solder freezes and cools to room temperature, the cells should bend under the influence of the thermal coefficient expansion mismatch. The ultimate objective is to predict this curvature theoretically and then, by determining the modulus of rupture of the gallium arsenide itself, extend the theory to predict the temperature at which failure should occur. It should be noted that much evidence exists for this phenomena occurring in silicon solar cells. In the case of silicon, however, the solder backing is applied at lower temperatures and the weak link in the assembly is not the silicon, but its contact layers; these tend to peel off the cell.

Measurements were made of the deflection of the center of "free" cells. The deflection is perpendicular to the 2-cm dimension of the cell and is measured from a hypothetical line joining the ends of the cell. Thirteen cells were measured with the following results.

Cell No.	Deflection (inches)	Cell No.	Deflection (inches)
H-349	0.00123	H-267	0.00118
H-350	0.00000	H-268	0.00108
H-346	0.00055	H-271	0.00022
H-365	0.00150	H-270	0.00004
H-356	0.00164	H-269	0.00020
H-354	0.00105	H-283	0.00065
H-357	0.00072	mean	0.00077

In addition, two cells with contact layers but with no solder were measured. Their deflections were 0.00007 and 0.00045 inches. The theoretically computed deflection of the cells falls very close to these observations. Some difference would exist because of solder and cell-thickness variations and because of the unknown properties of

the solder at high temperature, i.e. because of creep, the cooling solder may induce no stress in the cell until some temperature below its freezing point. The equations used to predict this curvature include the solder thickness to essentially the fourth power. This can explain the wide variation in measured deflections.

(6) Exposure of Cells with RTV-60 to Low Temperatures

Two cells were then placed in the chamber and brought down to minus 80°C; neither cracked. They were then mounted on a 40-mil thick aluminum panel with fresh RTV-60, and put back in the temperature chamber. As the temperature was lowered the cells were checked at minus 57°C and minus 75°C; they did not crack. When the temperature was finally lowered to minus 97°C, one of the two cells cracked.

(7) Thermal-Vacuum Cycling Tests of GaAs-Cell Panel

(a) Introduction

A test program was conducted to determine the effect of cycling a GaAs solar-cell panel. The temperature limits of the panel and the temperature profile during heating and cooling simulated that of a 240 nautical-mile apogee and 110 nautical-mile perigee polar orbit, with a minimum of 59 percent sun time.

An orbital period of 90 minutes results in a daytime of 52 minutes and night-time of 38 minutes.

The thermal response during the day is governed by the equation:

$$mc\frac{dt}{d\theta} = A_f \alpha_f S + (A_f e_f \phi_{fE} + A_B e_B \phi_{B-E})_\mu + (A_f \alpha_f \phi_{fE} + A_B \alpha_B \phi_{B-E})_\rho$$
$$- A_B e_B \phi_{B-S} \sigma(T^4 - T_s^4) - \left[A_f e_f + A_B e_B (1 - \phi_{B-S})\right]\sigma T^4 \quad (1)$$

The thermal response at night is controlled by:

$$mc\frac{dT}{d\theta} = (A_f e_f \phi_{f-E} + A_B e_B \phi_{B-E})_\mu - A_B e_B \phi_{B-S} \sigma(T^4 - T_s^4)$$
$$- \left[A_f e_f + A_B e_B (1 - \phi_{B-S})\right] \sigma T^4 \quad (2)$$

Where:

the mass of the panel (0.1 lb.) is m;

the specific heat of the panel (361 watts per pound per °k) is c;

the areas of front and back surface (9 in^2 ea) are A_f, A_B;

the emissivity of front and back surfaces (0.75, 0.85) are e_f, e_B;

the absorptivity of front and back surfaces (0.9, 0.2) are α_f, α_B;

the solar constant (0.9 watts per square inch) is S;

the geometrical shape factors between the front and back surfaces to earth are ϕ_{f-E}, ϕ_{B-E};

the earthshine at orbit altitude is μ;

the shape factor between the back surface and the main satellite is ϕ_{B-S};

the temperature of main satellite is T_s;

the Stefan-Baltzmann constant is σ; and

the value of albedo at orbit altitude is ρ.

Because the solar panel is to be sun-oriented, the quantities ϕ_{f-E}, ϕ_{B-E}, and ρ are time dependent in a rather complicated manner and T_s is not a known quantity. Therefore, in this analysis, average values were taken for ϕ_{f-E}, ϕ_{B-E}, and ρ and the influence of the main satellite was neglected. Taking average values will result in a certain amount of variation in the temperature actually experienced from that calculated (approximately ±10°C). Neglecting the influence of the main satellite will cause a decrease in the maximum temperature during the day, since the main satellite will cut off part of the albedo and earthshine. This influence will be small, however, since the solar cell panel is mounted on a thin boom 10 feet away from the vehicle and thus the vehicle subtends a half angle of 12° while the earth subtends a half angle of 74°.

The day and night transient-response equation then becomes:

$$\text{Day:} \qquad mc \frac{dT}{d\theta} = C_1 - (A_f e_f + A_B e_B)\, \sigma T^4 \tag{3}$$

$$\text{Night:} \qquad mc \frac{dT}{d\theta} = C_2 - (A_f e_f + A_B e_B)\, \sigma T^4 \tag{4}$$

where C_1 and C_2 include the average earthshine and albedo impends. To further obtain a better approximation, C_1 was chosen at three places in the orbit during the day; at -45°, 90°, 135°. With these averages the equation becomes:

Day: $$\frac{dT}{d\theta} = 0.227 - 0.398\,\sigma T^4 \quad \text{for} \quad 0 \leq \phi \leq 45°$$

$$\frac{dT}{d\theta} = 0.232 - 0.398\,\sigma T^4 \quad \text{for} \quad 45° \leq \phi \leq 135°$$

Night: $$\frac{dT}{d\theta} = 0.227 - 0.398\,\sigma T^4 \quad \text{for} \quad 135° \leq \phi \leq 180°$$

$$\frac{dT}{d\theta} = 0.00478 - 0.431\,\sigma T^4$$

This temperature as a function of time (θ) was then calculated by using a numerical integration of the form:

$$T_{m+1} = T_m + \frac{dTn}{d\theta}\,\Delta\theta + \frac{d^2T_m}{d\theta^2}\,\frac{(\Delta\theta)^2}{2!}$$

Where it was finally decided after trial that $\Delta\theta$ = 120 sec. would give an accurate response. The result is shown in Figure 6.

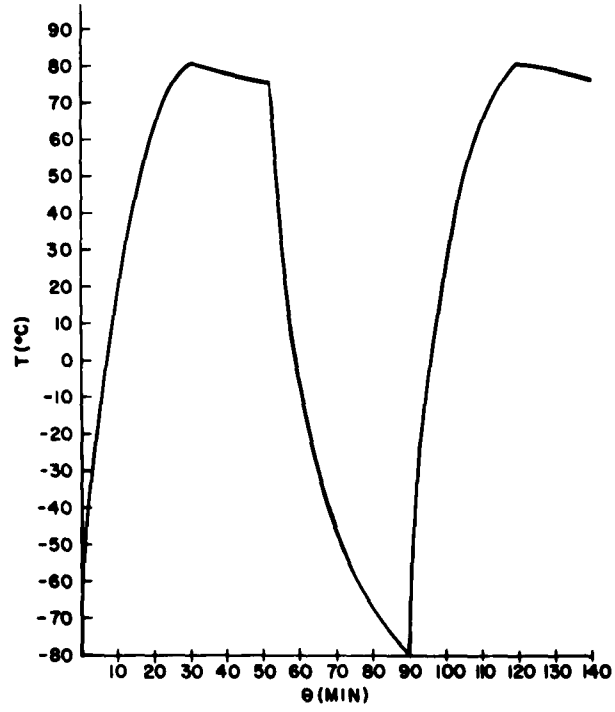

Figure 6. Calculated Response of GaAs Solar-Cell Panel

(b) Procedure

Three quartz lamps were mounted 4 inches apart in a cylindrical shroud 13-1/2 inches in diameter and 18 inches high. Hanging parallel to the three lamps was a 4-x-2-1/2-inch solar-cell panel approximately 4 inches from the lamps. During the test, liquid nitrogen flowed through the shroud maintaining a cold wall of minus 155°C or less. Micro switches were mounted on a temperature recorder with limits set at minus 80°C and plus 80°C. These switches controlled relays which turned the lamps off and on when the appropriate limits were reached as shown in Figures 7 and 8.

Thermocouples were placed on the board and cell face in various locations to determine temperature gradients through the board during the transient state. These thermocouples were attached to the surface with aluminized nylon tape.

(c) Results

A comparison of the actual and calculated response of the panel shows a "flat" in the calculated response. This "flat" was left out during the actual testing of the panel for it was felt that the information obtained during the steady state was not of any significant importance in determining the effect of thermal cycling.

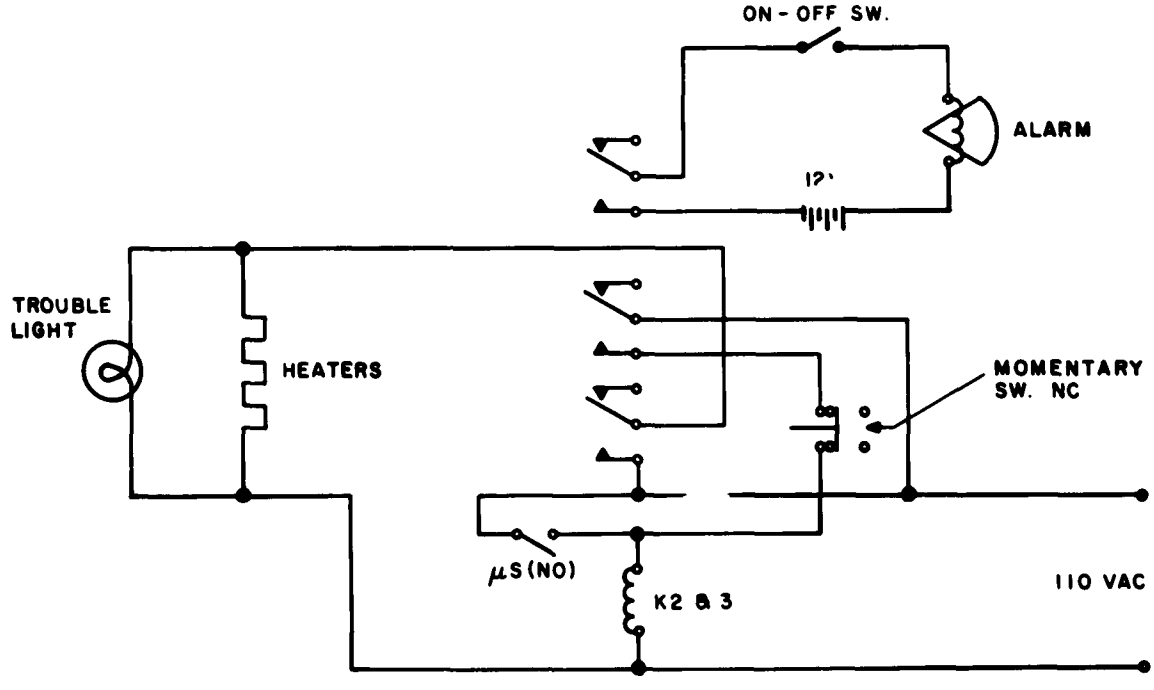

Figure 7. Low Limit Protection Circuit

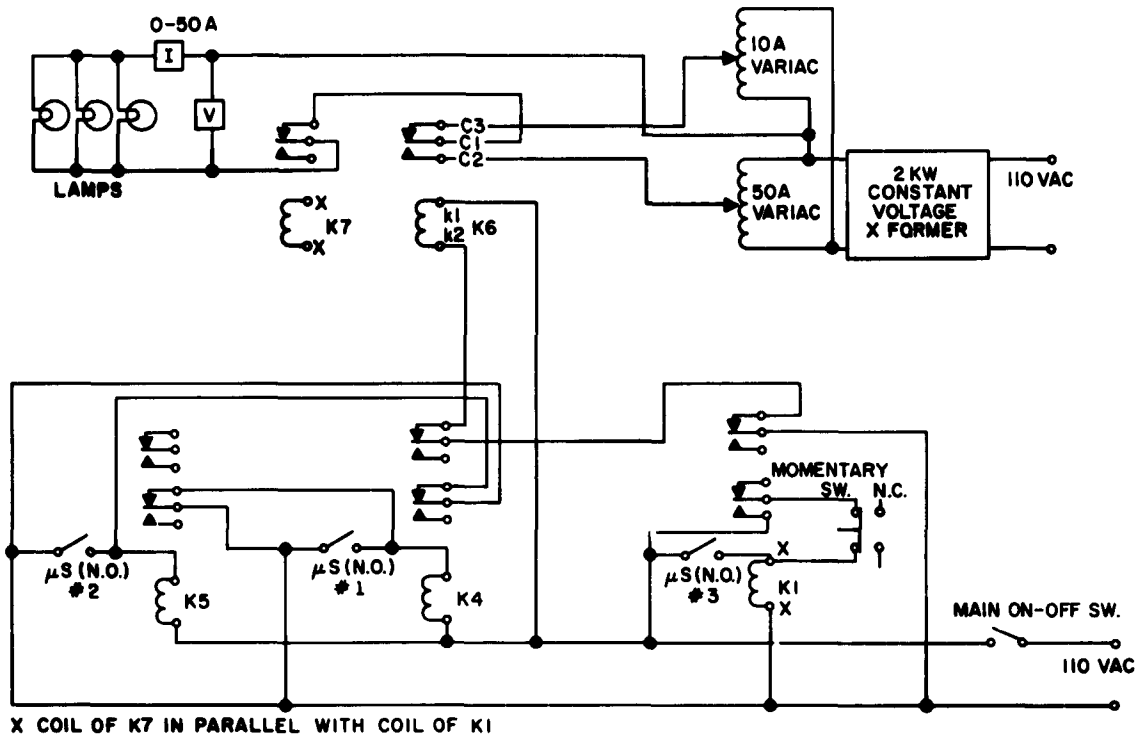

Figure 8. High Limit Protection Circuit

Figure 9 presents the heating-cooling curves for typical cell surface temperature of the long and short cycle. The cycles varied in length due to the variation in flow of liquid nitrogen and to the variation in lamp voltage. The shortest and longest cycles the panel was exposed to were 44 and 72 minutes, of which 14 minutes of the short cycle was heating, and 35 minutes of the long cycle was heating. The panel was subjected to a total of 38 cycles with an average total cycle time of 57 minutes.

The calculated rate of temperature change for the first two minutes of heating was 20°C per minute, where the actual response during test for the same period was 30°C per minute.

(d) Calibration

A panel 6 by 5 inches was divided into 30 one-inch-square blocks. The short-circuit current was read in the center of each of these blocks with a standard solar cell for various lamp voltages. The voltage was varied in 5-volt steps from 25 to 60 volts, and it was found that there existed a maximum of 10 percent intensity variation in the solar-cell-panel area of 4 by 2-1/2 inches.

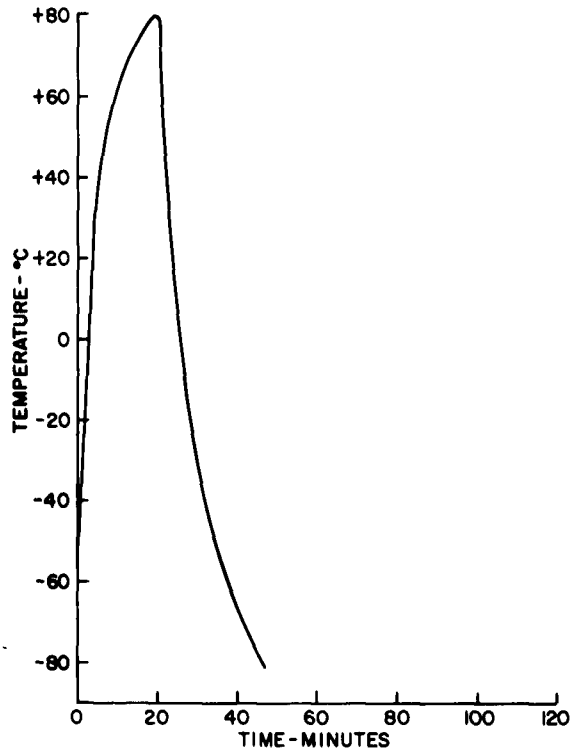

Figure 9. Actual Response of GaAs Solar-Cell Panel

(e) Re-Evaluation and Modification of the Panel

Upon completion of the thermal-vacuum cycle test of the solar-cell panel, it was decided to restrict the temperature limits the panel will experience. A new temperature range of minus 15°C to plus 82°C was accomplished by changing the total mass of the panel from 0.1 to 0.2 pounds, investigating the emissivity of the back of the panel, and by revised estimate of the earthshine input during the nighttime portion of the orbit. The temperature-time profile (shown in Figure 10) of the panel was calculated in a slightly different manner for the 0.2 pound board. Using the same equations as previously:

The thermal response during the day is governed by

$$mc\frac{dt}{d\theta} = A_f \alpha_f S + (A_f \epsilon_f \phi_{f\text{-}E} + A_B \epsilon_B \phi_{B\text{-}E})_\mu + (A_f \alpha_f \phi_{f\text{-}E} + A_B \alpha_B \phi_{B\text{-}E})_\rho \quad (1)$$

$$- A_B \epsilon_B \phi_{B\text{-}S} \sigma (T^4 - T_s^4) - \left[A_f \epsilon_f + A_B \epsilon_B (1 - \phi_{B\text{-}S})\right] \sigma T^4 \text{ , and}$$

the thermal response at night is controlled by:

$$mc\frac{dT}{d\theta} = (A_f e_f \phi_{f-E} + A_B e_B \phi_{B-E})_\mu - A_B e_B \phi_{B-S}\,\sigma(T^4 - T_s^4) - \left[A_f e_f + A_B e_B (1 - \phi_{B-S})\right]\sigma T^4 \qquad (2)$$

where the mass of the panel (m) is 0.2 lb. and all other parameters are unchanged from paragraph (7) (a).

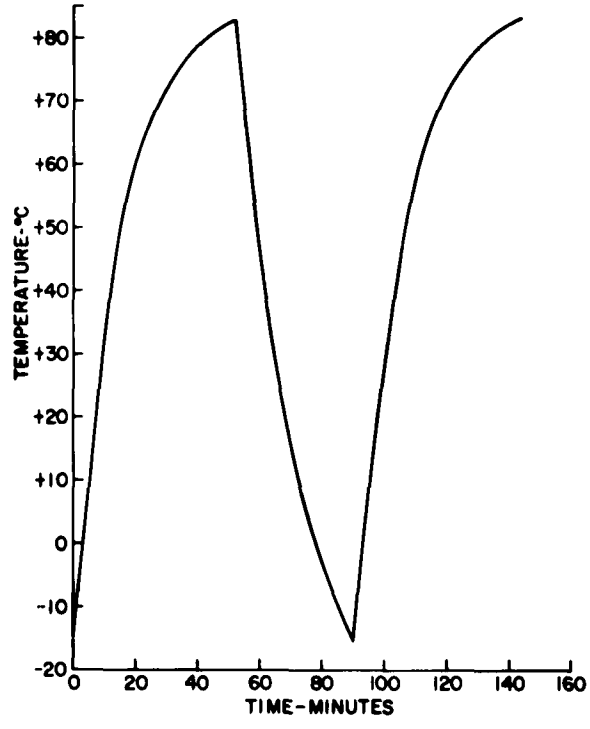

Figure 10. Calculated Temperature Response of 0.2-Lb. Panel

An exact solution of equation (1) may be found by setting the earthshine, albedo and direct solar inputs equal to D, neglecting the influence of the main satellite as previously stated.

Then $$D - A\left\{e_f + e_B\right\}\sigma T^4 = mc\,\frac{dT}{dt} \qquad \text{(day)}.$$

Rearranging and integrating:

$$t = \frac{m}{2C_D^3}\left\{\tanh^{-1}\frac{T}{C_D} + \tan^{-1}\frac{T}{C_D}\right\} \qquad \text{(Daytime equation).}$$

Limits of integration

When $t = 0$ $\quad T = T$

$t = t_D$ $\quad T = T_f$

$$(t_D)\left(\frac{2C_D^3}{m}\right) = \left[\tanh^{-1}\frac{T_f}{C_D} + \tan^{-1}\frac{T_f}{C_D}\right] - \left[\tanh^{-1}\frac{T_i}{C_D} + \tan^{-1}\frac{T_i}{C_D}\right]$$

(Daytime equation).

Let the nighttime input N include only the earthshine, neglecting the effect of the main satellite; then from equation (2)

$$N = \sigma A\left\{e_f + e_B\right\}T^4 = mc\frac{dT}{dt}$$

Solving for t =

$$t = \frac{\rho}{2C_N^3}\left\{\tan^{-1}\frac{T}{C_N} - \frac{1}{2}\ell n\frac{T - C_N}{T + C_N}\right\} \qquad \text{(Nighttime Equation)}$$

Limits of integration:

$t = t_D$ $\quad$ when $T = T_f$

$t = t_0$ (orbit time) $\quad$ when $T = T_i$

or

$$t_N = \frac{\rho}{2C_D^3}\left\{\tan^{-1}\frac{T_i}{C_N} + \frac{1}{2}\ell n\frac{T_f - C_N}{T_f + C_N} - \left(\tan^{-1}\frac{T_f}{C_N} + \frac{1}{2}\ell n\frac{T_i - C_N}{T_i + C_N}\right)\right\}$$

Nighttime equation $\quad$ where t_N = night orbit time = $(t_0 - t_D)$

Evaluation of the shape factors for day and for night was accomplished by plotting the values at various positions around the orbit, drawing a smooth curve through these values, and finding the area under the curve as the average shape factor. The results of this may be seen in Figure 11.

As a result of the difficulty encountered during the instrumentation of the panel it has been decided to design a circuit that will utilize the silicon wafer as a temperature-measuring device. A circuit has been designed (shown in Figure 12) such that the wafer will have the same output as a copper-constantan thermocouple. Thus the wafer, which is bonded just behind a solar-cell, can be used in conjunction with a standard copper-constantan temperature recorder to control the temperature limits achieved by the panel during the test cycles.

Investigation of the back-surface finishes for a 0.2-pound panel gave the following results:

α	e	T_{max}	T_{min}
0.2	0.85	+82°C	-15°C
0.15	0.7	+90°C	- 8°C
0.08	0.1	+115°C	+14°C

(8) Conclusions

The following tentative conclusions can be drawn, based on experimental data and analysis:

1. Gallium arsenide cells, as presently made, with or without soldered leads, can withstand thermal cycling from plus 80°C to minus 80°C with a temperature rate of change of 30°C per minute.

2. Materials suitable for silicon cell arrays are not suitable for GaAs cell arrays when subjected to the thermal conditions specified in 1 above, because of the inherent weakness of GaAs as compared with silicon.

3. Experimental data and analysis indicate that with proper choice of array materials, GaAs solar cells on a panel can be made to withstand temperature limits above 80°C and below 15°C, and a rate of temperature change in excess of 11°C per minute.

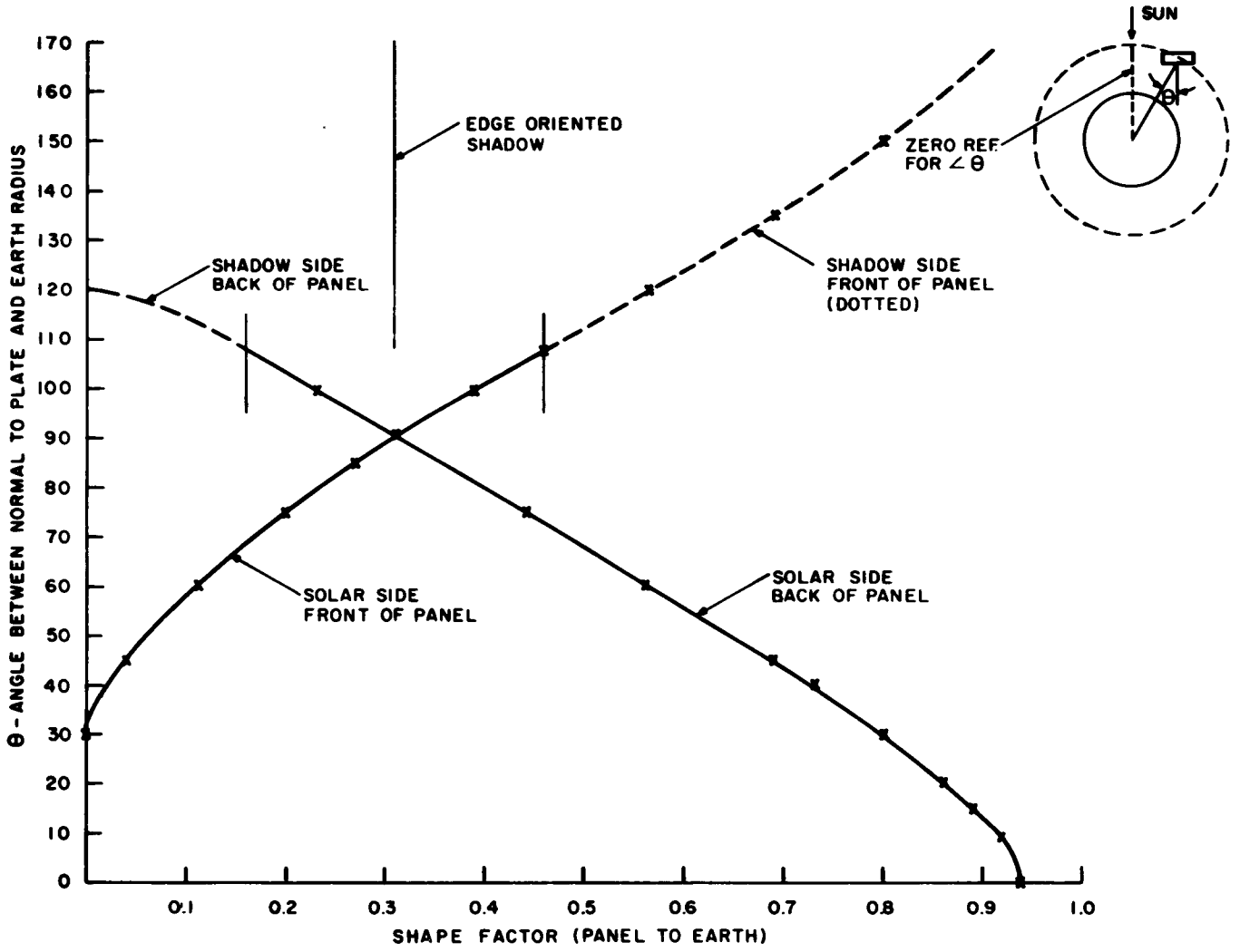

Figure 11. Shape Factor (ϕ_{Be}) versus Angle Between Normal to Plate and Earth Radius

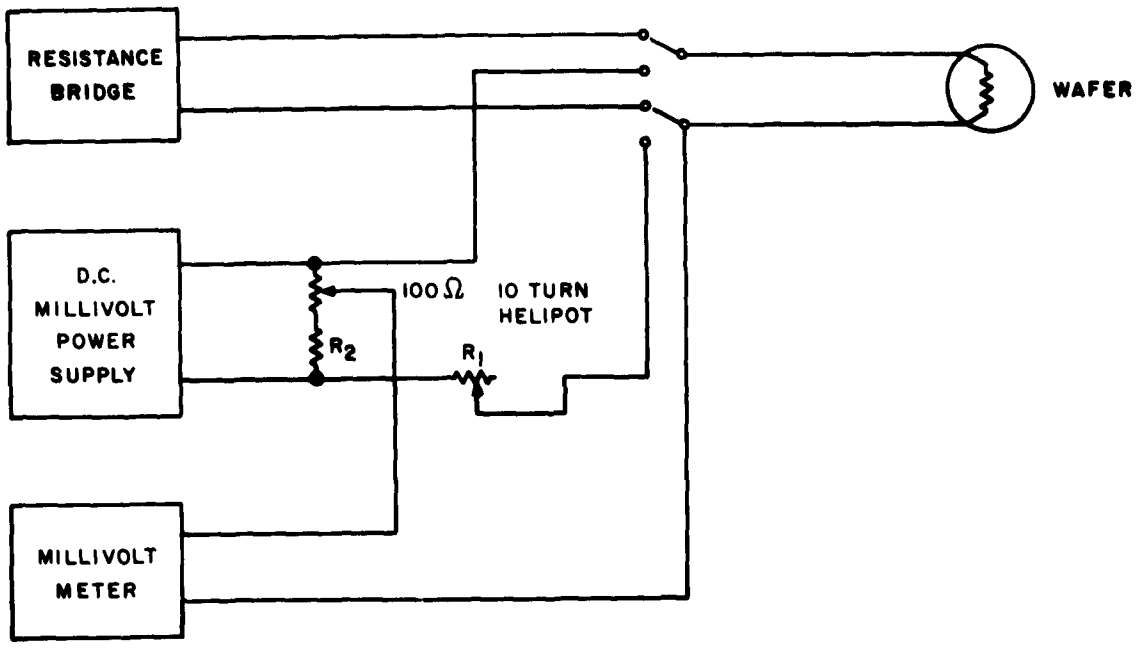

Figure 12. Circuit for Use of Silicon Wafer as Temperature-Measuring Device; Schematic Diagram

4. The inherent weakness of GaAs can be overcome by designing a proper combination of solder patterns and/or thickness and cell thickness. By this means, GaAs cells on a panel can be fabricated to withstand more severe temperature limits and temperature-time profile than plus 82°C to minus 15°C and 11°C per minute.

5. The power-to-weight ratio for the present orbital panel is 1.65 watts per pound. This ratio can be significantly increased by additional effort in this area.

As noted previously, these conclusions are tentative and more work is required in these areas in order to positively establish the limits of a GaAs cell solar panel.

4. Adhesive Work

The RTV-60 silicone-rubber adhesive, used to mount cells on arrays built to date, has successfully withstood all environmental tests. In addition, its history

is well known since it is used on a number of other types of solar-cell arrays. In light of this, no further adhesive-study work is contemplated for the orbital panels unless subsequent qualification tests indicate otherwise.

5. Soldering Techniques

Three techniques have been successfully used to date. The first is a straightforward application of conventional techniques with two exceptions; no flux is used and, to minimize thermal cracking, soldering-iron temperatures are reduced to a minimum. This method used 63/37 eutectic tin-lead solder and is hereafter called "low-temp" soldering. A tentative specification has been generated covering the technique; yields have been about 90 percent with the balance lost due to thermal cracking.

The second technique is the same as above except that the cell is placed on a hot plate at 100°C to 120°C and the soldering is done there. For approximately 30 cells done this way, thermal cracking has been eliminated.

The third technique is the same as the second except that the hot plate is at 200°C to 220°C and the solder used is the same composition as that on the cell back, i.e., 95.5 percent lead, 2.0 percent indium, 1.5 percent silver, and 1.0 percent tin. This is called "high-temp" soldering. Thermal cracking has been virtually eliminated by this process.

Figures 13 through 15 show another measure of soldering success. The differences between the soldering techniques (as far as short-circuit-current change are concerned) may be statistically significant. Additional samples are required in order to make a positive statement in this regard. The physical significance is not as yet understood. The other parameters appear to show no significant difference. One point that should be noted is the spread of the short-circuit soldering degradation data in Figure 15. This is simply explained by the characteristics of the current-voltage (I-V) curves; the measured parameter (voltage at 20 ma.) is in the region of the average maximum power point. The slope of the curve in this region is changing rapidly and in addition there are differences in the shape of the I-V characteristic from cell to cell. Accordingly, depending on the efficiency and shape of curve, small changes from the short-circuit current valve may produce small or large changes in voltage.

Peel tests have been conducted on "low-temp" connections. In all but a few cases, the cell ruptured, or occasionally, the lead wire failed. As previously reported, there were however, a few cases where the silver "P" strip peeled. Neglecting these few cases, the tests indicate that the gallium arsenide cells should present no problems with peeling of contact layers during temperature cycling. The interesting fact here is that in performing peel tests on silicon cells, failure almost invariably occurs by peeling of the same contact layer that peels during temperature cycling. This lends credence to peel testing as a measure of the ability to withstand thermal cycling.

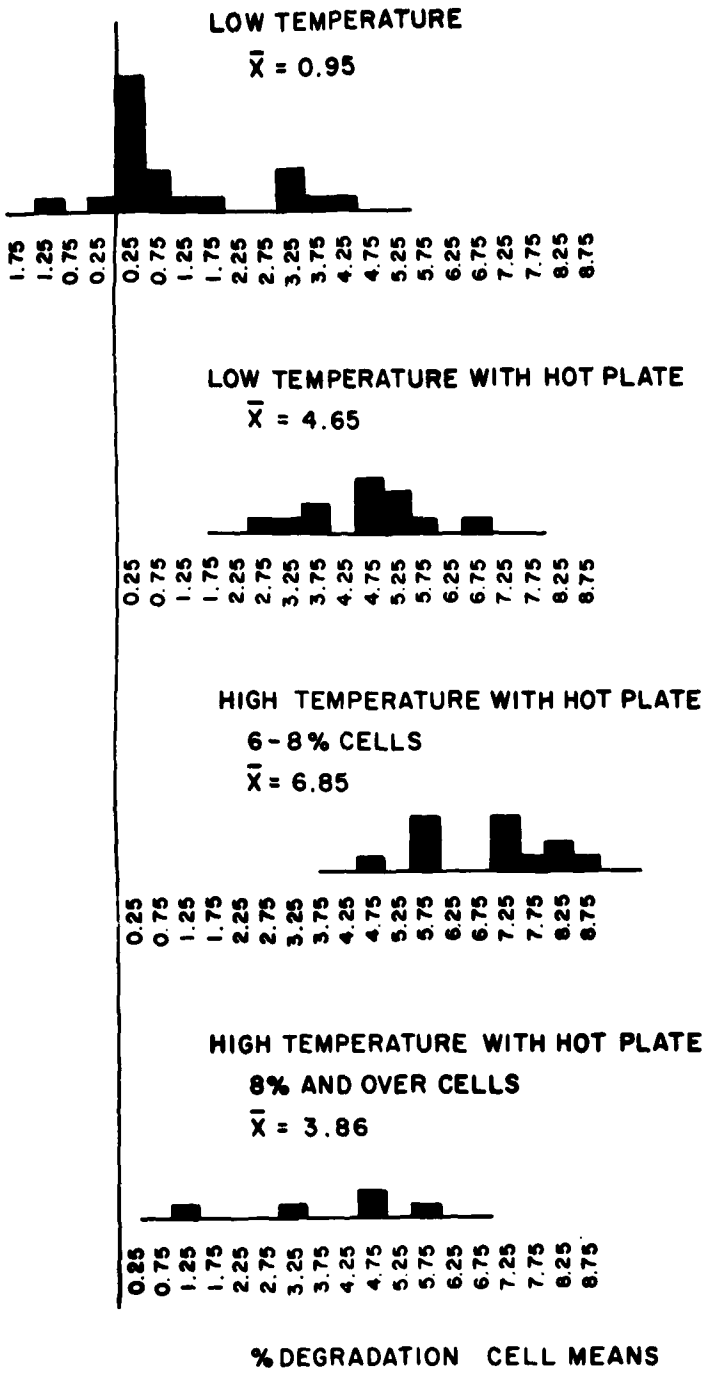

Figure 13. Soldering Degradation (Short-Circuit Current)

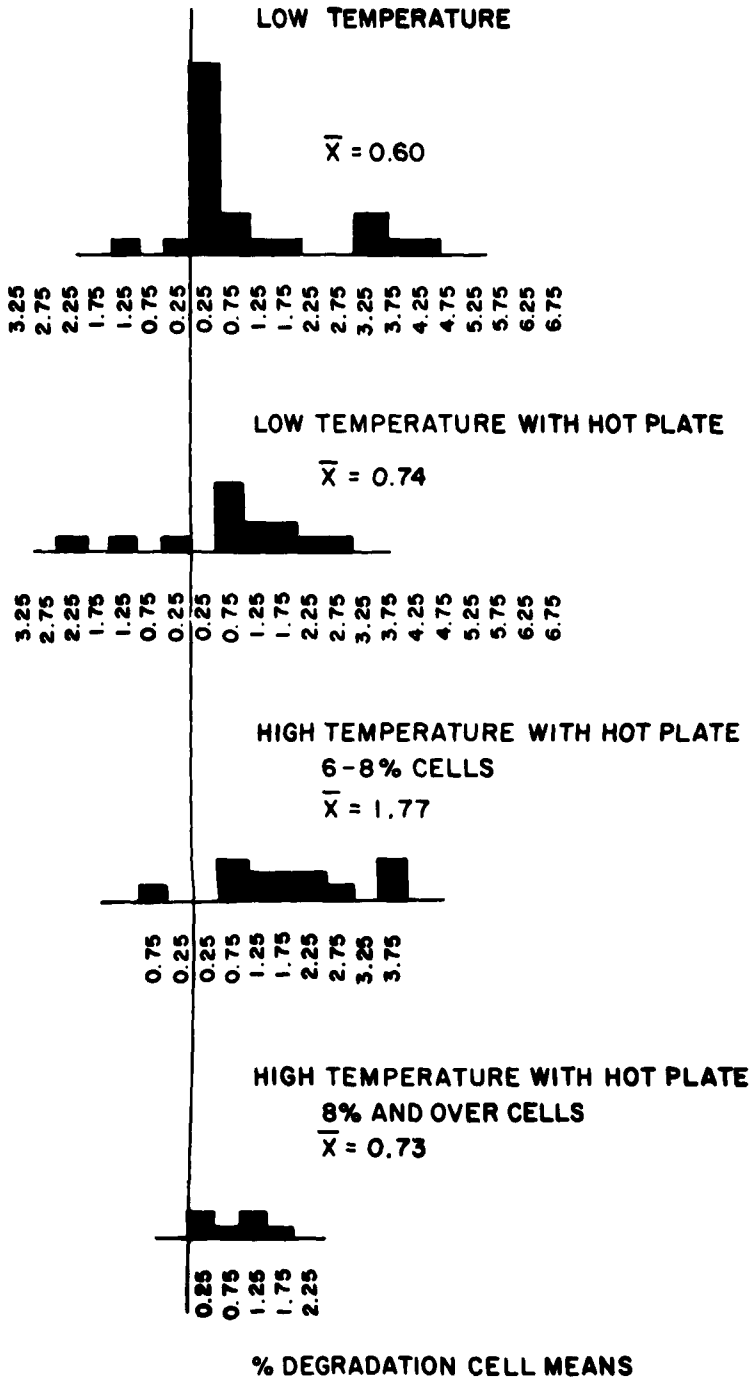

Figure 14. Soldering Degradation (Open-Circuit Voltage)

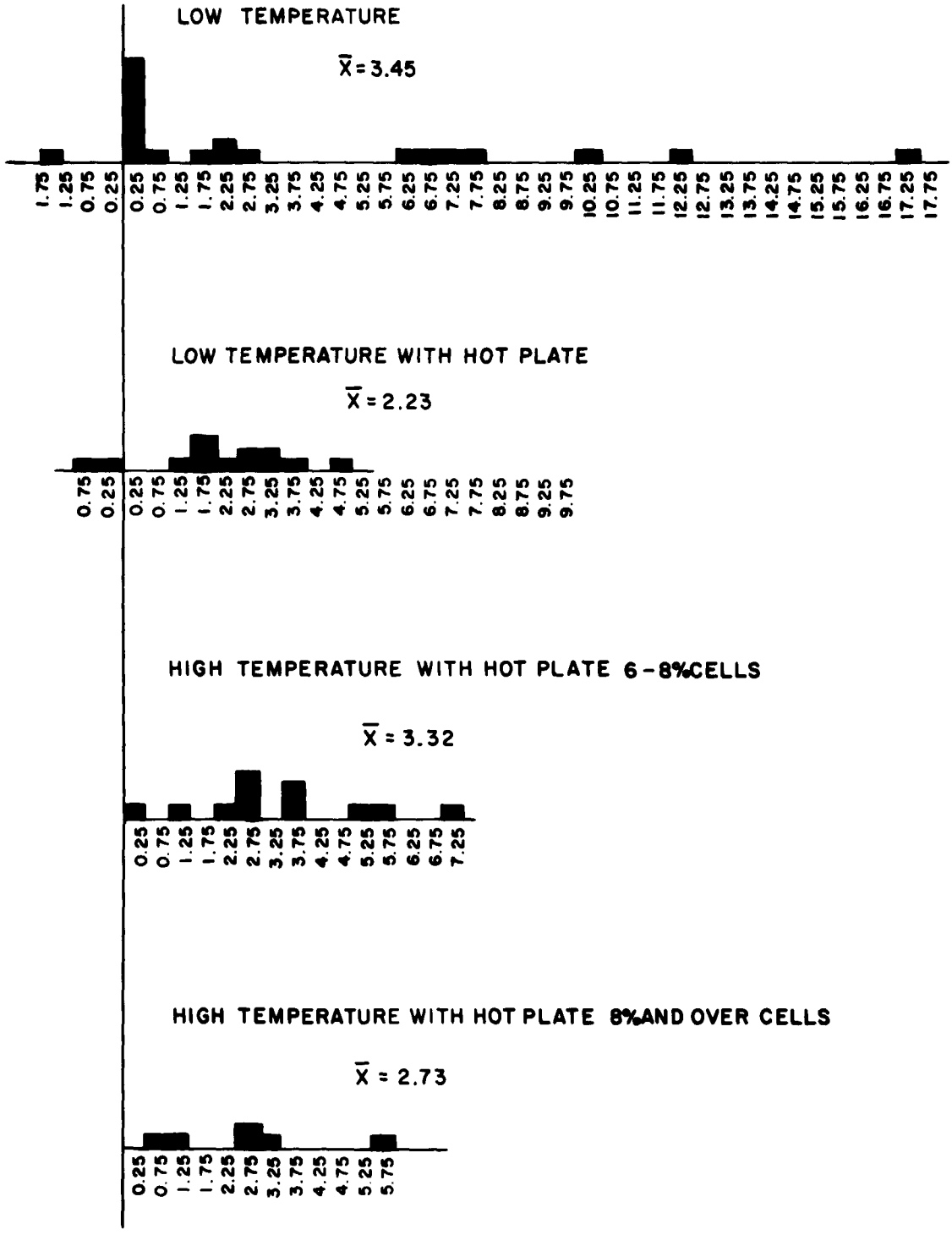

Figure 15. Soldering Degradation (Voltage Change at 20 ma.)

One possible anomaly has been detected to date. In either high- or low-temp hotplate soldering of cells with efficiencies less than 8 percent, thermal cracking has been completely eliminated. Approximately 75 cells have been done this way. To date, ten 8-percent cells have been high-temp soldered. Two of these have thermally cracked. It is not as yet clear whether this is pure chance, an inadvertent change in soldering procedure, or whether this is in some way associated with high efficiency. Additional samples are required in order to draw a definite conclusion.

C. Radiation Testing

1. Electron Irradiation

a. Introduction

Gallium arsenide (GaAs) and silicon (Si) n-on-p solar cells were irradiated with 0.8- and 5.6-Mev electrons in the continuing study of the effect of particle irradiation on these devices. The experiments were performed on the RCA 1-Mev Van de Graaff generator and the 6-Mev linear accelerator at the plant of Ethicon Products, Somerville, N.J. The conditions of operation for the experiments are listed in Table III.

TABLE III.

OPERATING CONDITIONS OF ELECTRON IRRADIATIONS

Parameter	0.8 Mev Experiment	5.6 Mev Experiment
Machine	1-Mev Van de Graff	6-Mev Linear Accelerator
Ambient Condition	Vacuum $\leq 2 \times 10^{-5}$ mm Hg	Air
Cell Position Relative to Beam	Perpendicular	Perpendicular
Beam Current	Steady; Maximum value of 0.23 μ a over area of 0.63 cm^2	Pulsed. Pulse width: 5 μ s; Pulse repetition rate: 400 cps. Average current: 10μ a over area of 26.1 cm^2
Maximum Temperature Rise in Cell During bombardment	80°C	60°C (estimated)

The measurements made included the sunlight efficiency and spectral response before and after bombardment as well as during the experiment. The light source consisted of an incandescent lamp, a filter of one inch of water with 7/16-inch of heat-absorbing glass, and eight interference filters spanning the spectral range of from 1.25 to 3.06 Mev. Sunlight measurements were also made during the 0.8-Mev experiment to check the effectiveness of the filtered incandescent source in predicting the performance in sunlight.

b. Description of the Cells

The silicon (Si) cells were of the n-on-p variety, obtained from the RCA Semiconductor and Materials Division (SM & D) at Mountaintop, Penna. The gallium arsenide (GaAs) cells came from the SM & D at Somerville, N.J.

The initial properties of these cells are listed in Table IV; the Si cells are designated by the prefix MT and the GaAs cells by S.

c. Results of the 0.8-Mev Run

These results are expressible in terms of the maximum power output of the cells versus flux, and the critical flux (ϕ_c) required to reduce the power output by 25 percent. The spectral response curves were not analyzed to yield the outer-space response inasmuch as previous work has shown that outdoor measurements are a good indication of outer-space response.

Another objective of this experiment was to compare the response obtained from the filtered incandescent light (with the one-inch of water and 7/16-inch of heat-absorbent glass) with that observed in sunlight during the tests. Inasmuch as the sun position at this time of year is far from normal with respect to the test area, measurements with the cells horizontal (required because the Laboratory pyrheliometer is a horizontal detector) are subject to errors of 10 to 20 percent. A further comparison was therefore based upon the initial measurement made earlier and final measurements made after bombardment; these measurements were made with the normal-incidence pyrheliometer at the Astro-Electronics Division (AED) of RCA. These readings, together with the curve obtained from the filtered incandescent source, were used to predict the sunlight performance. A comparison of the various measurements (in terms of the critical flux), as well as the performance of GaAs and Si cells, is given in Table V. All the cells listed in Table IV are not listed in Table V since certain of them broke or otherwise changed, preventing further analysis.

TABLE IV.

INITIAL PROPERTIES OF SOLAR CELLS

Cell No.	Initial Sunlight Efficiency (%)	Electron Irradiation
MT-0	10.2	0.8 Mev
MT-J4	10.5	0.8 Mev
MT-265A	10.1	0.8 Mev
MT-4A	9.7	0.8 Mev
MT-13A	9.1	0.8 Mev
S79-A	8.2	0.8 Mev
S12A	8.4	0.8 Mev
S14HA	8.2	0.8 Mev
S14HC	8.3	0.8 Mev
S164#1	-	0.8 Mev
MT-I	10.2	5.6 Mev
MT-5B	9.2	5.6 Mev
MT-11B	9.5	5.6 Mev
S12B	8.0	5.6 Mev
S79B	8.4	5.6 Mev
S14HB	7.8	5.6 Mev

TABLE V.

CRITICAL FLUX OF GaAs AND Si CELLS

Cell No.	ϕ_c (e/cm^2)		
	Filtered Incandescent Data	Sunlight Measurements During Bombardment	Initial and Final Sunlight Measurements
MT-J4	1.0×10^{15}	5.4×10^{14}	1.1×10^{15}
MT-4A	9.3×10^{14}	9.3×10^{14}	1.3×10^{15}
MT-13A	1.2×10^{15}	6.2×10^{14}	1.4×10^{15}
S79A	1.5×10^{15}	-	1.1×10^{15}
S12A	1.4×10^{15}	-	1.1×10^{15}
S14HC	1.0×10^{15}	8.5×10^{14}	1.0×10^{15}

There is good agreement between the various values of ϕ_c, particularly for the filtered incandescent data and for the initial and final sunlight measurement. The ϕ_c obtained from the sunlight measurements during bombardment is generally lower than that from the filtered incandescent data which is not usually the case. However, the sunlight measurements may be in error by 10 to 20 percent because of the large incidence angle of the sun's rays. The data in Table V is sufficiently significant, nevertheless, to warrant further comparisons between the filtered incandescent light and sunlight.

The relative power outputs of Cells No. MT-J4 and S14HC are shown in Figures 16 and 17 and illustrate the performance with the different light sources. The data from the filtered incandescent source is reasonably consistent with the sunlight data.

A comparison of power outputs from a Si cell and a GaAs cell is illustrated in Figure 18. The curves are based on the initial and final normal-incidence measurements in sunlight; they do not cross over primarily because the GaAs cell is less efficient. However, even if the GaAs cell were of the same efficiency as the Si cell, their performance would only be comparable up to flux values of 10^{15} electrons per square centimeter; at higher values, the Si cell would be superior because of its more gradual decrease in power output.

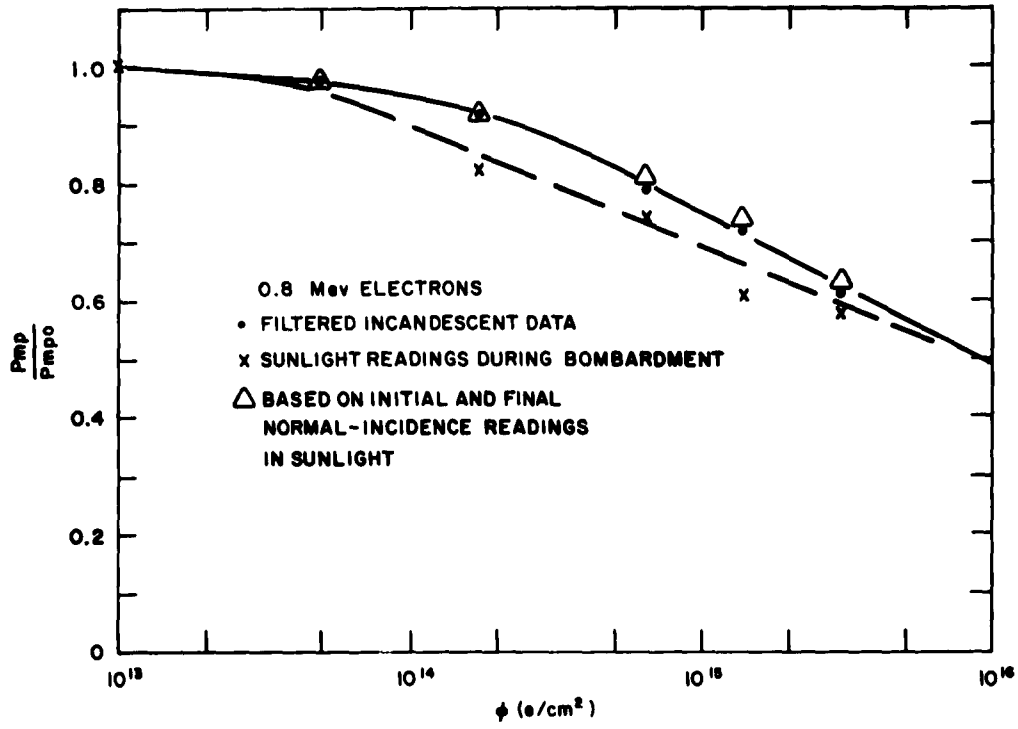

Figure 16. Comparison of Relative Power Output and ϕ for Cell No. MT-J4

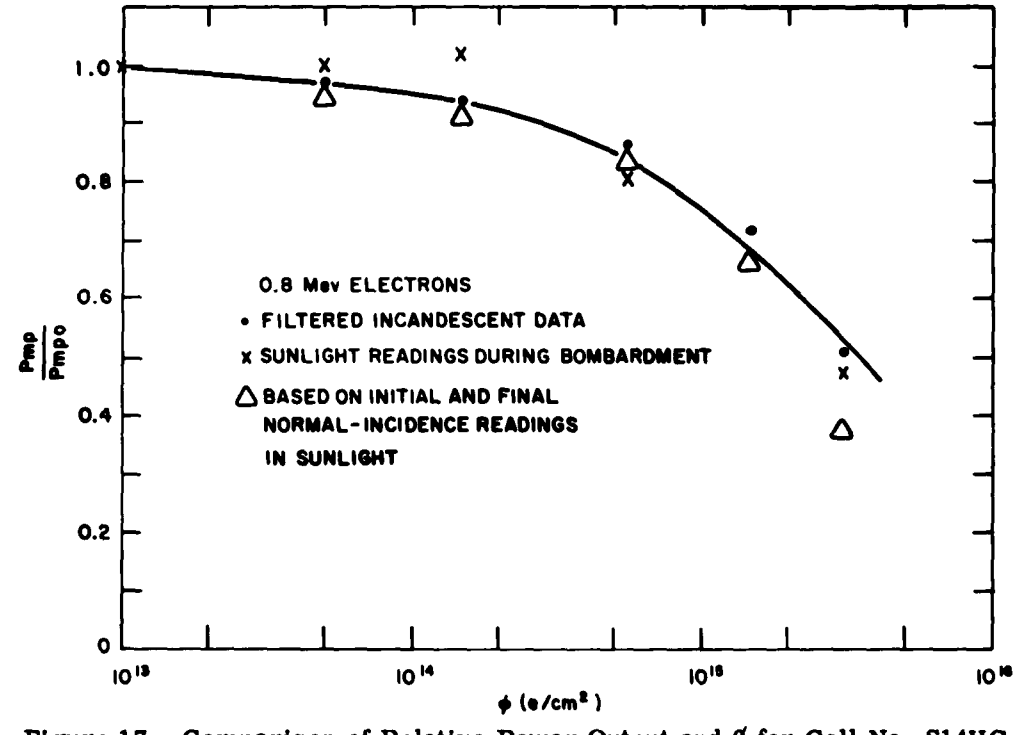

Figure 17. Comparison of Relative Power Output and ϕ for Cell No. S14HC

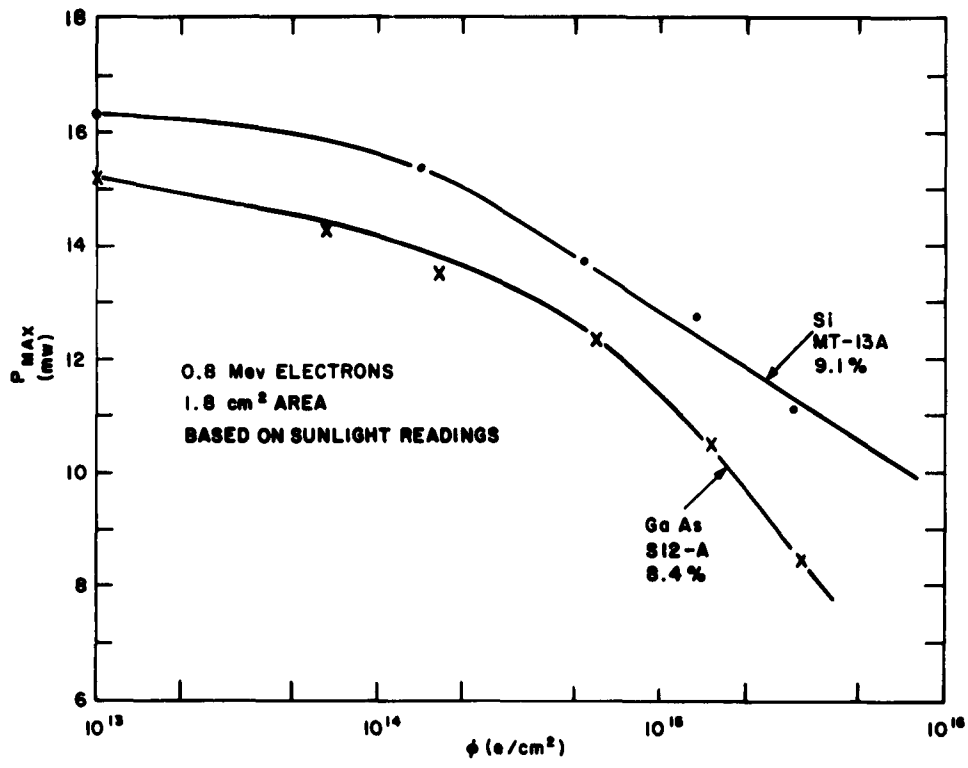

Figure 18. Comparison of Power Output and Flux for GaAs and Si Cells

The change in these cells as a result of the total flux (ϕ_T) is shown in Table VI in terms of the ratio of the final values of output power and short-circuit current to the initial values. The data is based on the final values measured at normal incidence in sunlight.

The percentage of decrease in the normalized power output of the Si cells per decade of flux in the linear region of the semi-logarithmic plots averaged 22 percent for sunlight and 25 percent for filtered-incandescent light. These values are comparable with those found by other workers but differ from the values reported for the 17.6-Mev proton irradiation. The inference is reinforced that annealing occurred in the 17.6-Mev run.

A comparison of the above results was made with the results of experiments conducted over a year ago on experimental GaAs and Si n-on-p cells. The conclusion at that time, in agreement with the present results, was that the GaAs and Si cells were comparable in radiation resistance to 0.8 Mev electrons. However, the average ϕ_c (based on filtered-incandescent-light data) was 2.3×10^{16} electrons per square centimeter for GaAs cells and 6.2×10^{15} electrons per square centimeter for Si cells with one-ohm-per-centimeter base material. (See Reference 1). The difference in these values of ϕ_c from the present ones is ascribed to improvements in both cells.

TABLE VI.

RATIO OF FINAL TO INITIAL VALUES BASED ON SUNLIGHT MEASUREMENTS

Cell No.	ϕ_T (e/cm^2)	I_f/I_i (%)	P_f/P_i (%)
MT-0	3.0×10^{15}	71	62
MT-J4	3.0×10^{15}	73	64
MT-4A	2.8×10^{15}	77	68
MT-13A	2.9×10^{15}	70	68
S79A	3.2×10^{15}	53	50
S12A	3.3×10^{15}	64	56
S14HC	3.0×10^{15}	46	38

For example, the smaller ϕ_C in present GaAs cells may be due to a larger minority-carrier lifetime and/or a larger constant (C) relating the fluence and lifetime (τ) as follows:

$$\tau = \frac{\tau_0}{1 + C \tau_0 \phi} ,$$

where τ_0 is the initial lifetime. To separate these two effects, the effective energy required to create an electronhole pair (which is subsequently collected) was determined for an old experimental cell and a current cell, using 25- to 35-kev electrons. The value for the experimental cell was 120 electron volts per collected pair (typical of values in the past) while that of the present-day cells is 42 electron volts per collected pair. The effective energy required to create an electron-hole pair, which is collected, is inversely proportioned to the sum of the diffusion lengths on both sides of the junction. Present-day cells have a total diffusion length three times larger than the experimental cells; consequently, the lifetime is improved by a factor of 10.

The lower ϕ_C found in present-day cells cannot, however, be completely explained on the basis of the improved lifetime; this parameter will only account for a factor of two to three. An increase in the value of the constant relating lifetime and flux by a factor of five must therefore be postulated, signifying the presence of another defect whose presence was not previously seen.

The ϕ_C of the experimental cell was in excess of 4.6×10^{15} electrons per square centimeter in support of the contention that the characteristics of GaAs cells have changed.

d. Results of the 5.6-Mev Run

Measurements made on the cells during this portion of the experiment were substantially the same as in the previous portion. Values for ϕ_c based on filtered incandescent light, and on initial and final sunlight are listed in Table VII. The two values of ϕ_c are in rather close agreement.

The average decrease in power output per decade of flux for the normalized semilogarithmic plots for the Si cell power output is 23 percent for the filtered incandescent light and sunlight data. Figure 19 compares the power output of the Si and GaAs cells as a function of flux; the curves are based on the initial and final sunlight measurements. The GaAs cells are shown to be clearly superior with greater power from 10^{13} to 10^{15} electrons per square centimeter; ϕ_c is larger for GaAs cells than for Si cells by a factor of 10. An interesting fact is that the general behavior shown in Figure 19 agrees with that obtained in the 17.6-Mev proton irradiation tests.

The change in these cells because of total irradiation is listed in Table VIII; the data are expressed in ratios of final to initial values of power output and short-circuit current in sunlight.

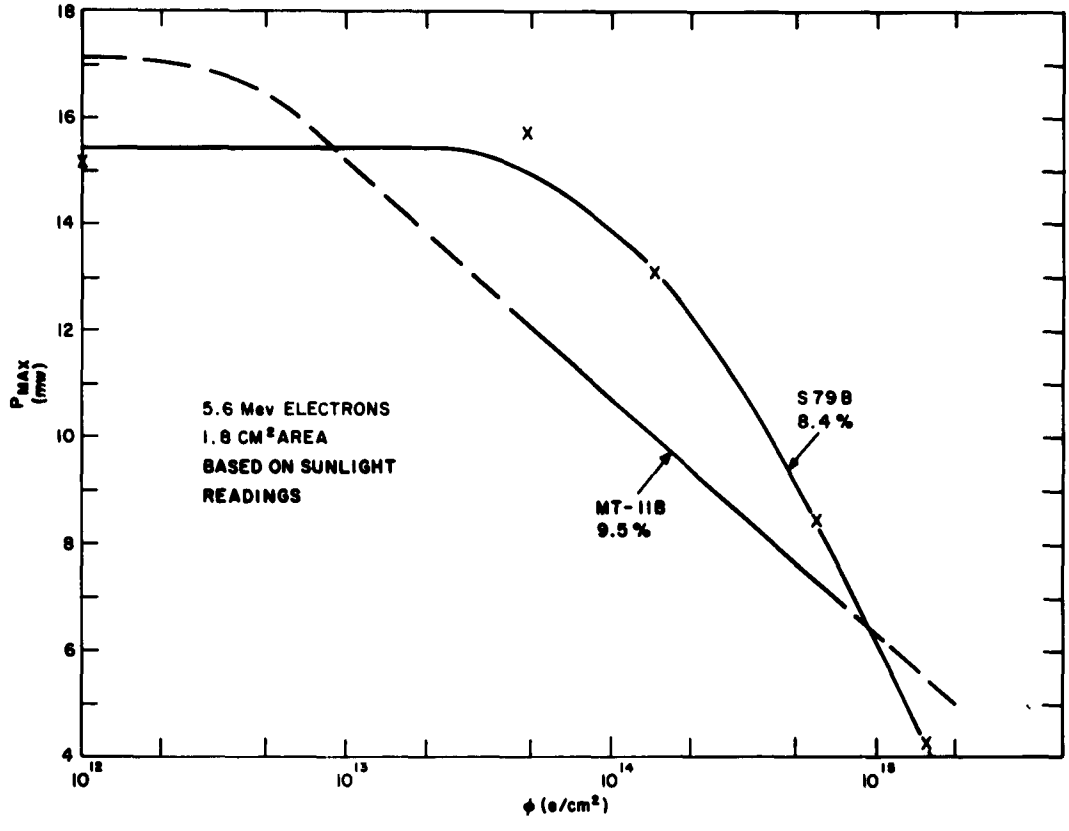

Figure 19. Comparison of Power Output and Flux for GaAs Cells

TABLE VII. ϕ_c FOR 5.6-MEV RUN

Cell No.	ϕ_c (e/cm^2)		
	Filtered Incandescent Light	Sunlight	
MT-I	3.0×10^{13}	3.0×10^{13}	Horizontal
MT-5B	1.1×10^{13}	6.0×10^{12}	Final Sunlight
MT-11B	4.3×10^{13}	3.1×10^{13}	Measurement
S12B	2.8×10^{14}	2.7×10^{14}	Normal Incidence
S79B	3.1×10^{14}	3.0×10^{14}	Final Sunlight
S14B	2.7×10^{14}	2.3×10^{14}	Measurement

TABLE VIII. CHANGES ARE TO TOTAL BOMBARDMENT, BASED ON SUNLIGHT MEASUREMENTS

Cell No.	ϕ_T (e/cm^2)	I_f/I_i (%)	P_f/P_i (%)
MT-I	6.2×10^{14}	53	45
MT-5B	6.2×10^{14}	55	40
MT-11B	6.2×10^{14}	47	43
S12B	1.6×10^{15}	38	28
S79B	1.6×10^{15}	32	28
S14HB	1.6×10^{15}	38	27

e. Discussion of Results and Conclusions

The conclusions arrived at as a result of the experiments are as follows:

(1) GaAs and Si cells are comparable in radiation resistance to 0.8 Mev electrons for fluxes of up to 10^{15} electrons per square centimeter; above this, Si cells are superior by virtue of the more gradual decrease in power output with increase in flux. The ϕ_c for GaAs is 1.1×10^{15} electrons per square centimeter and for Si 1.3×10^{15} electrons per square centimeter, based on sunlight measurements.

(2) The properties of present-day GaAs cells are superior to those of a year ago; specifically, the minority-carrier lifetime is one order of magnitude higher.

(3) The relative performance of GaAs and Si cells is accurately determined although there is some question concerning the flux scale in the 5.6-Mev experiment; the GaAs cells are ten times better in radiation resistance than the Si cells. Based on sunlight measurements, ϕ_c is 2.7×10^{14} electrons per square centimeter for GaAs cells and 3×10^{13} electrons per square centimeter for Si cells. However, the Si cells will deliver more power for flux levels greater than 10^{15} electrons per square centimeter.

(4) The Si cells degraded 40 times faster at 5.6 Mev than at 0.8 Mev; the GaAs cells degraded only four times faster.

(5) The performance of the cells in sunlight is reasonably close to that in the filtered incandescent light; this is to be expected inasmuch as the use of heavy filtering causes an incandescent light spectrum to approach the sunlight spectrum.

Those of the items listed which merit further discussion are the ones concerning the relative performance of GaAs and Si cells and the greatly enhanced rate of damage in the Si cells at 5.6 Mev.

It has been established that GaAs cells are initially superior to Si n-on-p cells when irradiated with 1.8, 17.6 and 95.5 Mev protons. (In all cases, the Si cells eventually outperform the GaAs cells by virtue of their more gradual drop in power output with increase in flux.) It is intuitively expected, therefore, that the initial superiority would also be evident in the case of electron irradiation. This expectation was realized in the case of the 5.6-, but not the 0.8-Mev experiment. Questions arise as to whether this behavior is attributable to a distribution of defects or to the type of defect introducted.

The rapid damage in Si cells at 5.6 Mev compared to that at 1 Mev also requires examination since it was not expected and since it is a factor in the comparison of GaAs and Si cells. The cross-section for producing a primary defect in Si has been computed by H. Flicker using the relativistic McKinley-Feshback formula. The cross-section is 65 barns for 1-Mev, and 76 barns for 6-Mev electrons. Furthermore, the numbers of secondary defects per primary displacement is around 1.3 for 1-Mev, and 2.1 for 6-Mev electrons. Consequently, the damage rate at 6 Mev should only be twice as large as that at 1 Mev, but a factor of forty is obtained. The question resolves itself then as to whether this increased rate is due to the introduction of another defect or to failure of reciprocity, i.e. the resulting damage depends not only on the integrated dosage but also on the magnitude of the beam intensity. This latter item merits consideration because of the pulsed nature of the 5.6-Mev irradiation. Conceivably, if non-reciprocal effects were occuring in the Si and not in the GaAs, much of the relative advantage of GaAs at 5.6 Mev could disappear if the irradiation were performed at lower beam intensities.

The failure of reciprocity in Ge has been noted for 0.5-Mev electrons when the peak beam current exceeds 20 ma per square centimeter. At a peak current of 200 ma per square centimeter, the damage rate was seven times higher than that at 20 ma per square centimeter. (See Reference 3). A comparison of the peak-current density in the 5.6-Mev experiment to the values quoted above is difficult since each of the main 5 μs pulses itself consisted of a large number of microwave pulses. A lower limit to the peak current density given by the duty ratio of the 5 μs pulse is 0.19 milliamperes per square centimeter. The upper limit is probably less than 20 milliamperes per square centimeter because the peak power required from the machine would then be in excess of 3 megawatts. Hence, based on the experience with Ge, it is doubtful that non-reciprocity can be invoked to explain the high damage rate in Si cells for 5.6-Mev electrons.

The other possibility for explaining the high rate is the introduction of another defect. Such a defect may be the divancy, an intrinsic defect consisting of two vacant, nearest-neighbor, lattice sites. (See Reference 4). Although it is produced at a rate of approximately 5 percent of the vacancy-production rate for 1.5-Mev irradiations, it is more efficiently produced at higher electron energies (Reference 4). Further experimental work at various electron energies is required to resolve these questions concerning the damage rate in Si solar cells.

The differences seen in the relative rates of damage in GaAs and Si solar cells with electron and proton irradiation may result either from the damage distribution effects or the introduction of different defects in electron and proton irradiations. The damage produced by high-energy protons is expected to be uniform throughout the active regions of the GaAs and Si cells.* The damage is also more complex than in the

*The active region extends from the surface to a depth of 150μ in Si cells and no more than 5μ in the GaAs cells.

case of an electron irradiation since the protons can transfer more energy to the lattice atoms. Even in the case of electron irradiations, however, approximately uniform damage is expected in the active regions of these cells provided the electron energy is much greater than the threshold energy for damage. For example, Flicker has shown that the damage rate in Si due to 0.5-Mev electrons decreases by only a factor of two for the first 100μ of Si (Reference 5). The change in rate will be even smaller for 0.8-Mev electrons. Almost no change in rate can be expected in GaAs cells since the active region is so small. For any energy above the threshold, the damage will be effectively uniform in GaAs cells. Also arguing against distributional effects is the results of the 1.8-Mev proton irradiation. These protons have a range of approximately 2 mils in Si and less in GaAs, yet the GaAs cells are more radiation-resistant than the Si cells by a factor of 10 or more. The possibility is indicated that different defects in the proton and electron irradiations are responsible for the observed performance of GaAs and Si cells.

f. References

(1) Final Triannual Report, Semiconductor Photovoltaic Conversion, DA36-039-SC-87417; Report Date: November 30, 1961. (Signal Corps, U.S.A.)

(2) F. Seitz and J. S. Koehler "Displacement of Atoms During Irradiation," Solid State Physics 2, Academic Press, Inc. (1956), p. 382.

(3) P. Baruch, "The Use of the Electron Accelerator in Solid State Physics," Nuclear Inst. and Meth. 11, 196(1961).

(4) J. W. Corbett and G. D. Watkins, "Silicon Divancy and Its Direct Production by Electron Irradiation," Phys. Rev. of Letters 7, 314(1961).

(5) H. Flicker, Private Communication.

2. 1.8-Mev Proton Irradiation

Three GaAs cells were irradiated with 1.8-Mev protons at Ohio State University. The initial efficiency, critical flux (ϕ_C), and ratio of final to initial values of short-circuit current and efficiency as a result of the total irradiation (ϕ_T) are listed in Table IX. All of the solar-cell parameters are based on sunlight measurements.

The critical flux is three to four times smaller for 1.8-Mev protons than for 17.6-Mev protons. A reduction is expected because of the energy dependence of the damage

TABLE IX. RESULTS OF 1.8-MEV PROTON IRRADIATION

Cell No.	η_i (%)	ϕ_c (Protons/cm^2)	ϕ_T (Protons/cm^2)	$\frac{I_f}{I_i}$ (%)	$\frac{\eta_f}{\eta_i}$ (%)
91B	7.9	1.4×10^{12}	1.8×10^{13}	17	8
76B	8.1	4.3×10^{12}	1.8×10^{14}	1	0.2
46HB	8.7	1.6×10^{12}	6.4×10^{13}	15	6.7

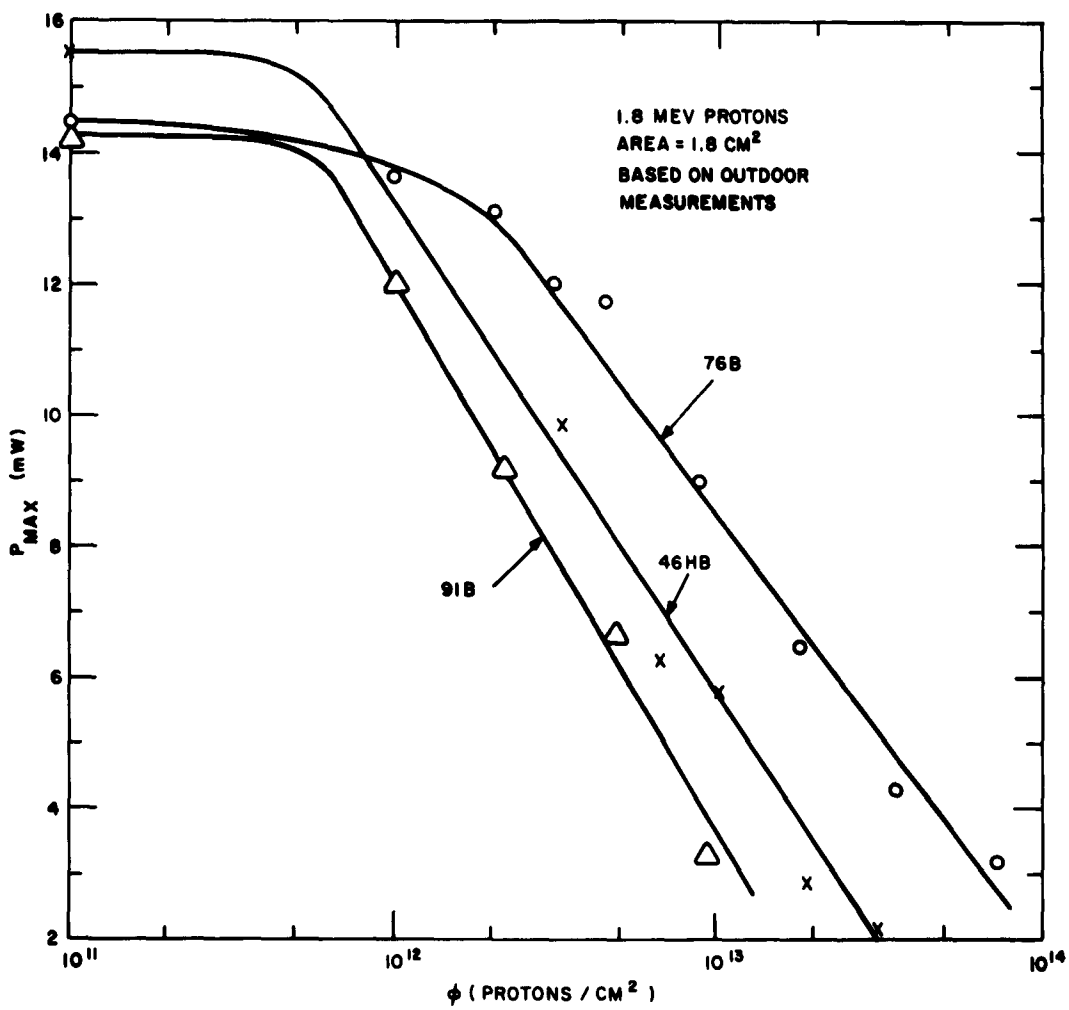

Figure 20. Plot of P_{max} versus Flux for GaAs Cells (1.8-Mev Proton Irradiation)

introduction rate and also because of the defect distribution. Protons with 1.8-Mev energy are far less penetrating than 17.6-Mev protons, hence damage is produced closer to the surface where the predominant photovoltaic response of GaAs occurs. The reduction in ϕ_c is somewhat smaller than expected; however, a reduction by a factor of ten would be implied, for instance, by a 1/E dependence of the introduction rate such as found in Si cells.

The defect-distribution effect is evident from the drastic reduction in short-circuit current and efficiency as a result of the total irradiation. This effect is more evident in the efficiency degradation which includes both the short-circuit current and open-circuit voltage degradations. Obviously there was a sizeable drop in open-circuit voltage.

Curves of the maximum power output as a function of flux are shown in Figure 20. Although Cell 76B was irradiated with 1.8 Mev protons, its curve is representative of the results obtained at 17.6 Mev. By comparison, the curves for the other two cells show the effect of the defect distribution and energy dependence of the introduction rate.

D. Thin-Film Gallium Arsenide Investigation

1. Introduction

The work described in this section was undertaken in an attempt to fabricate thin, single crystal films of gallium arsenide (GaAs) on a germanium (Ge) substrate as a possible use as a major cost reduction technique for the GaAs solar cell. Since the active part of a solar cell extends only for several microns below the surface, a GaAs layer no more than 10 microns thick supported by a much thicker, lower cost, single-crystal wafer of Ge should be a feasible device structure. The Ge would also act as a low-resistance ohmic contact.

The initial technical approaches to this work center on an evaluation of methods for depositing epitaxial films of GaAs on Ge, techniques for producing the desired doping structure, and studies of the resultant photovoltaic and surface contacting properties.

2. Methods of Producing GaAs Films

Three methods for producing single-crystal films of GaAs on Ge are currently being used. The first, shown in Figure 21, utilizes a stream of hydrogen (H_2) gas which passes over a source of GaAs at a temperature of about 900°C. Arsenic enters the flowing H_2 quite readily, while the Ga is most probably carried along as GaO by traces of oxygen or water vapor in the H_2.

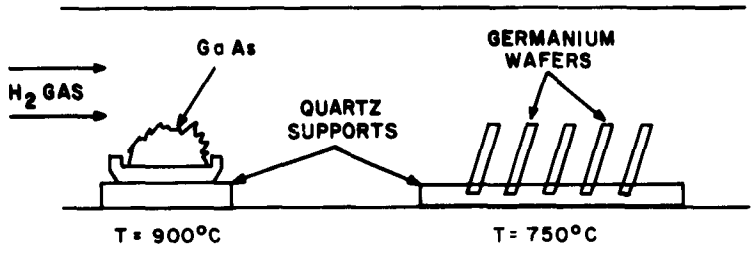

Figure 21. Schematic Drawing of Apparatus for Forming GaAs Films on Germanium Using GaAs as the Source Material

The GaAs deposits on the Ge at about 750°C. One serious drawback to this method is that the production rate is quite slow, most probably due to the distance between the source and the substrate. Film growth rates are about 1/2 micron per hour; several days are required for a run and only three to four wafers of Ge can be used in the apparatus at one time. The second method, as in Figure 22, involves the passage of gases over the elements Ga and As rather than over GaAs. Here, the H_2 stream flows over elemental As at one end of a quartz "Tee", a hyrdogen and bromine (Br) stream flows over elemental Ga at the other end of the "Tee" (the Ga thus being transported as Ga Br), while the formation of GaAs on the Ge takes place in the center stem of the "Tee". The temperatures are controlled separately at each region. The heaters are so designed that a constant-temperature region exists at the position of the Ga, As and Ge wafers. Bromine is used because preliminary tests have shown that it is purer and more easily controlled than anhydrous hydrogen chloride (HCl) which is more commonly used as the chemical reactant for this type of reaction. Preliminary runs have been made and have proven the apparatus to be satisfactory. The temperature of the As was 415°C, that of the Ga was 795°C and that of the Ge wafers was 595°C. Growth rates of the GaAs are about five to ten microns per hour.

The third method used successfully for growing GaAs films on Ge involves heating a flat wafer of GaAs in a graphite boat to temperatures of 850°C to 950°C. The Ga and As are transported in an H_2 atmosphere (by mechanisms essentially identical to those used in method 1) and deposit on the Ge wafer now situated much closer to the GaAs source. Layers can be grown at the relatively rapid rate of about 1 mil per hour.

3. Discussion of Results

Studies of appropriate doping structures and procedures have been found to be dominated by two facts. The first is that whenever Ga and As are deposited simultaneously on Ge, a thin degenerate p-type Ge layer is formed at the surface because Ga has the highest solubility of any impurity in Ge and diffuses much more

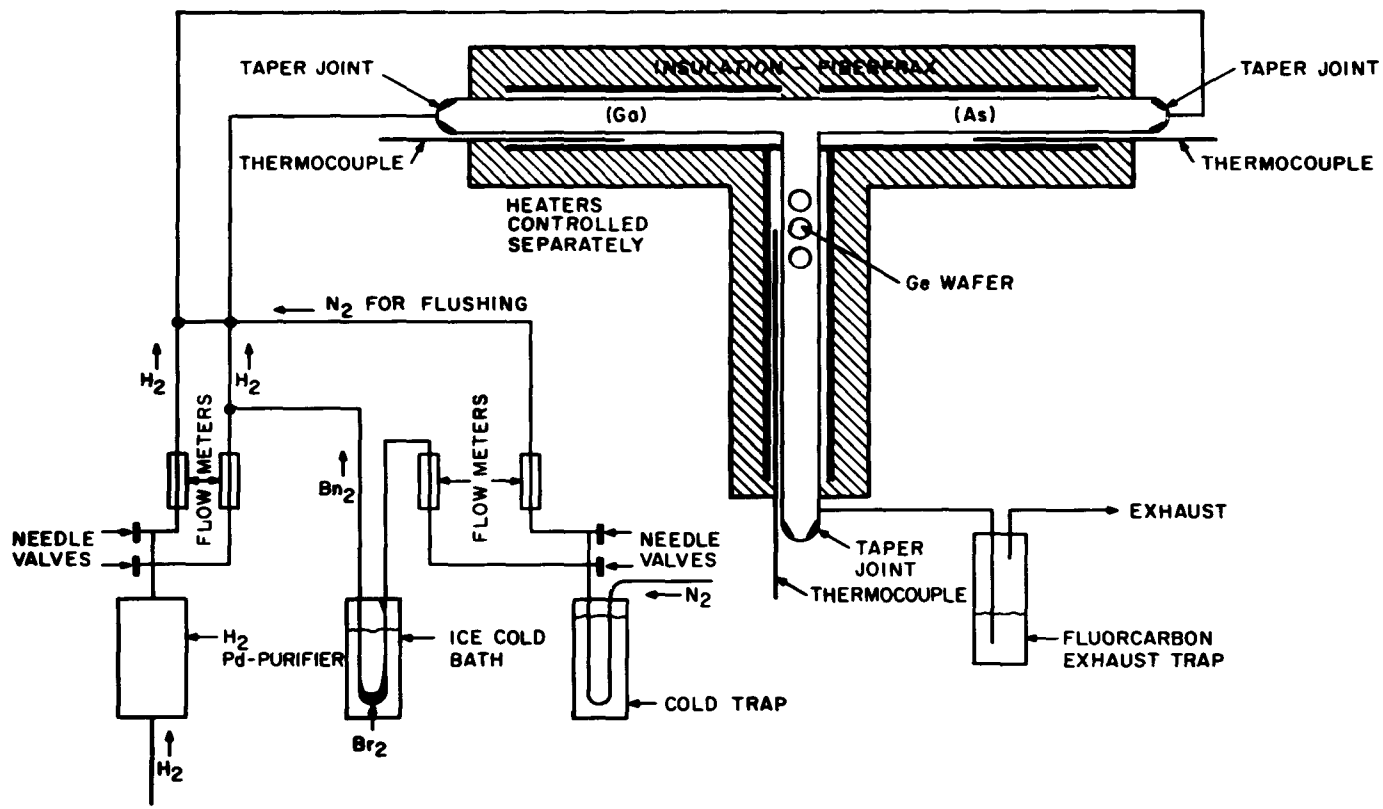

Figure 22. Schematic Drawing of Apparatus for Forming GaAs Films on Germanium Using the Elements (Ga and As) as Component Raw Materials

slowly than As. Thus, in order to avoid a junction in the Ge substrate or at the GaAs-Ge interface, p-type Ge (already degenerate) must be employed, and the GaAs in contact with the Ge must be p-type. This, in turn, dictates that the photovoltaic element in the GaAs film must be an n-on-p device. The second fact is that since GaAs and Ge are eutectic at 878°C, very serious limitations are placed on the diffusion temperature of the dopant impurity (and therefore the dopant impurity itself) available for achieving an appropriate doping structure. Thus, obtaining the appropriate doping during the film growth rather than afterward is important; our present work takes both these facts into account. For example, all our Ge substrate material is p-type, Ga doped, and has a resistivity of 4×10^{-4} ohm-centimeter.

Several GaAs single-crystal films ten to thirty microns thick have been prepared using the method illustrated in Figure 21. These have almost always been n-type, even when a p-type GaAs source has been used. Although some photovoltaic effects have been observed with these films (0.25-volt open-circuit voltage and 10 to 20 milliampere per square centimeter short-circuit current) the wavelength response of these effects begins at a photon energy of 0.68 ev, thus indicating that these are not due to junctions within the GaAs, but that at least one side of the photovoltaic element is Ge. Several GaAs films one to three mils thick have also been grown by the third method described. These films, too, are invariably n-type even when the source wafer of GaAs is heavily doped with Zn and Cd (10^{20} and 4×10^{18} atoms per cubic centimeter respectively). In order to study this lack of control over the doping of the films during growth, radioactive Zn^{65} and Cd^{115} are being used in tracer experiments. The very interesting initial results have shown that the amount of Zn or Cd in the deposited films is about 10^3 less than that in the source wafer.

In support of a program directed toward the fabrication of a solar cell consisting of a thin polycrystalline layer of GaAs on which a photovoltaic metallic contact is evaporated, metallic contacts to single crystal GaAs are being investigated. Such photovoltaic metallic contacts on single crystal n-type GaAs have been prepared using evaporated films of silver (Ag), platinum (Pt), and chromium (Cr). In order to obtain a useful photovoltaic response, such contacts must possess a relatively large barrier height (ideally approaching the bandgap). In addition, the metallic film must possess a high optical transparency simultaneous with a low electrical-sheet resistivity. For these reasons the measurements during this quarter have been confined to the determination of contact-barrier heights and current-voltage characteristics, the evaluation of the physical characteristics of the metallic film, and comparative photoresponse measurements using a focussed microscope lamp.

Three independent methods of measuring the contact-barrier height have been used. One is the differential capacitance method which, under proper conditions (Reference 1), provides an accurate measurement of the barrier height in terms of the voltage dependence of the inverse square of the barrier capacitance. This method is illustrated in Figure 23, for a Ag-GaAs contact. The barrier height may also be measured

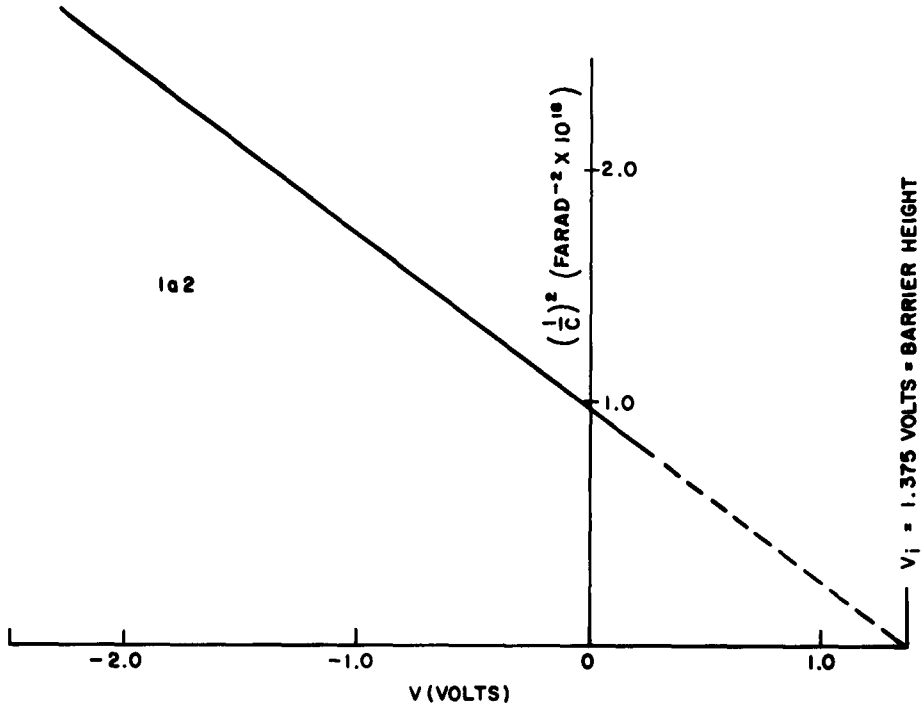

Figure 23. Plot of $(\frac{1}{C})^2$ versus Voltage for Ag-GaAs Contact

by measuring the wavelength dependence of the photoemission of electrons from the metal into the semi-conductor (Reference 2). However, since this method is accurate only over a restricted range of barrier heights, it has not been useful with the GaAs contacts prepared to date. The current-voltage characteristic of the contact provides yet another means by which to measure the barrier height. The current-voltage relation for a rectifying metal-semiconductor contact can often be described by the relation,

$$I = I_o (e^{-\frac{qv}{mkT}} - 1)$$

where I_o is the reverse saturation current. From a measurement of I_o and m, both of which are experimentally determinable constants, the barrier height of the contact can be calculated when the Fermi level in the semiconductor is known (Reference 3). This method is illustrated for the case of a Cr-GaAs contact in Figure 24.

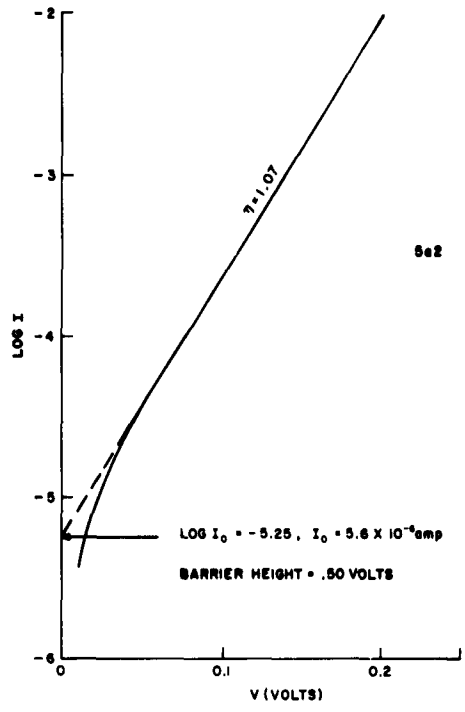

Figure 24. I-V Characteristic of Cr-GaAs Contact, Forward Bias

The barrier height of Ag contacts on single-crystal n-type GaAs has been found to be nearly as high as the GaAs bandgap, e.g. 1.4 ev. However, the contact characteristics are not easily reproducible. Furthermore, it has not been possible to produce an optically transparent Ag film while still maintaining a low electrical sheet resistivity. The barrier heights of Cr-GaAs contacts was measured to be approximately 0.6 volts. These contacts possessed very uniform and easily reproducible characteristics. They should therefore be of use in studying GaAs surface properties. One set of Pt contacts has been prepared: preliminary measurements indicated a barrier height of 0.6 to 0.8 volts. The Pt film was tough, semi-transparent, and highly conducting. Open-circuit voltages of 0.5 volts and short-circuit currents of 1.2 milliampere per centimeter have been measured for these contacts in indirect sunlight.

4. References

(1) A. M. Goodman, to be published in J. Appl. Phys., Feb. 1963.

(2) W. G. Spitzer, G. R. Crowell, M. M. Atalla, Phys. Rev. Letters, 8, 7, (1962).

(3) A. Van Der Ziel, Solid State Physical Electronics (Prentice-Hall, Inc. 1957).

II. WORK TO BE ACCOMPLISHED NEXT QUARTER

A. Gallium Arsenide Cell Development and Fabrication

Production of gallium arsenide cells is complete. No further work is contemplated in this area with the exception of the final report.

B. Array Design and Testing

Orbital panels are scheduled for completion. The 6-percent-array fabrication and testing will be completed. Work in the 10-solar-constant area will be completed.

C. Radiation Testing

No additional radiation-damage experiments will be conducted since work in this area has been completed.

D. Thin-Film Gallium Arsenide Investigation

Work in the future will emphasize the understanding and the bringing under control of film fabrication techniques and doping procedures. Experiments involving radioactive tracers will continue. Measurements of GaAs surface properties and metallic contacts, (both large and small area) will also continue.